

Article

Comparative Study on Boiling Heat Transfer Characteristics and Performance of Low-Temperature Heating System of R744 and Its Azeotropic Refrigerant

Dahan Sun ¹, Xin Zhang ², Zhongyan Liu ^{2,*} and Hao Zhang ²¹ School of Energy Science and Engineering, Harbin Institute of Technology, Harbin 150001, China² School of Energy and Power Engineering, Northeast Electric Power University, Jilin 132000, China

* Correspondence: llzzyy198584@126.com

Abstract: R744 is the most competitive and ideal natural refrigerant when flammability and toxicity are strictly limited. However, there are still some problems when it is applied to a heating system. For example, the discharge pressure of the system exceeds 10 MPa, it increases the cost of the system, and the cycle efficiency is also low. To solve these problems, this paper proposes to replace R744 by mixing R744 and ethane at a ratio of (77.6/22.4) to form an azeotropic refrigerant. At present, there is little research on R744 azeotropic refrigerant. Therefore, this paper first establishes the CFD model and compiles the UDF program to focus on flow boiling heat transfer characteristics, and then, it analyzes the performance of R744 and its azeotropic refrigerant in a low-temperature heating system. The results show that the heat transfer coefficient of R744 and its azeotropic refrigerant decreases with an increase in mass flux and increases with an increase in heat flux and saturation temperature; the heat transfer coefficient of azeotropic refrigerant is greater than R744; and there is no dryness under the same conditions. Under a given operating condition, there is a critical point that makes the performance of azeotropic refrigerant better than R744, and this critical point is related to the outlet temperature of a gas cooler, and the system discharge temperature of azeotropic refrigerant is significantly lower than that of R744. In conclusion, azeotropic refrigerant has certain advantages in heat transfer and system performance compared with R744, which will also play an important role in promoting the replacement of refrigerant in the future.

Keywords: R744; azeotropic refrigerant; COP; 2D model; boiling heat transfer; refrigerant replacement



Citation: Sun, D.; Zhang, X.; Liu, Z.; Zhang, H. Comparative Study on Boiling Heat Transfer Characteristics and Performance of Low-Temperature Heating System of R744 and Its Azeotropic Refrigerant. *Energies* **2023**, *16*, 1313. <https://doi.org/10.3390/en16031313>

Academic Editors: Huijin Xu and Guojun Yu

Received: 6 December 2022

Revised: 10 January 2023

Accepted: 19 January 2023

Published: 26 January 2023



Copyright: © 2023 by the authors. Licensee MDPI, Basel, Switzerland. This article is an open access article distributed under the terms and conditions of the Creative Commons Attribution (CC BY) license (<https://creativecommons.org/licenses/by/4.0/>).

1. Introduction

At present, most of the refrigerant used in refrigeration and heating products is synthetic refrigerant, which has greenhouse effect potential (ODP) and ozone layer destruction potential (GWP), which have serious impacts on the environment. The natural working medium R744 receives wide concern from the industry thanks to its good environmental characteristics; however, there are still some problems when it is applied to heating systems. For example, the discharge pressure of the system exceeds 10 MPa, it increases the cost of the system, and the cycle efficiency is also low. To solve these problems, many scholars mixed R744 with other refrigerants. The research on refrigerant involves mainly the mechanism of flow boiling and the performance of the whole system. There are many experiments but few simulations on the mechanism of flow boiling in tubes with R744, and the research on R744 azeotropic refrigerant has been even more rarely reported.

In terms of experiments, Grauso et al. [1] studied the flow boiling heat transfer characteristics of R744/R290 with mass ratios of 83.2/16.8 and 70/30, respectively, through a horizontal smooth tube. The result showed that the flow boiling heat transfer characteristics of R744/R290 were evaluated. Afroz et al. [2] studied the heat transfer and pressure drop characteristics of binary mixtures (mass ratios: 39/61 and 21/79, respectively) in a horizontal smooth tube. The result showed that the heat transfer performance of R744/dimethyl

ether was better than that of pure R744, and with an increase in the R744 mass ratio, the calculation formula was modified according to the experimental results. Onaka et al. [3] studied the evaporation heat transfer coefficients of pure dimethyl ether and a mixture of R744 and dimethyl ether (two mass ratios: 10/90 and 25/75, respectively) in a horizontal smooth tube with an inner diameter of 4.2 mm. The results showed that the heat transfer coefficient can be reduced by 20% for 10/90 and 48% for 25/75 by adding R744. Zhu et al. [4] studied the evaporation heat transfer characteristics of R744/R290 (75/25, 50/50, and 25/75) in a horizontal smooth microchannel pipe (inner diameter of 2 mm). The results showed that the heat transfer coefficient of the mixture is between R744 and R290, which is directly proportional to the ratio of R744 and inversely proportional to the evaporation temperature. Yun et al. [5] studied the flow boiling heat transfer of R744 in a horizontal tube with an inner diameter of 6 mm. The results showed that the heat transfer coefficient of R744 is on average 47% higher than that of R134a under the same conditions. Zhao et al. [6] studied the boiling heat transfer of R744 at low temperatures in a horizontal tube with an inner diameter of 4.57 mm. The results showed that the boiling heat transfer coefficient of R744 is much lower at low temperatures but that it increases with vapor quality. Oh et al. [7] studied the flow boiling heat transfer and pressure drop characteristics of R744 in a horizontal tube with an inner diameter of 4.57 mm. The results showed that the boiling pressure drop of R744 increased with an increase in the mass flux and decreased with an increase in the saturation temperature. Yun et al. [8] studied the convective boiling heat transfer coefficients and dry-out phenomena of R744 in rectangular microchannels whose hydraulic diameters ranged from 1.08 to 1.54 mm. The result showed that the hydraulic diameter decreases from 1.54 to 1.27 mm and from 1.27 to 1.08 mm at a heat flux of 15 kW/m² and a mass flux of 300 kg/m²·s, respectively, and that the heat transfer coefficients increase by 5% and 31%, respectively. Ozawa et al. [9] studied the flow pattern and boiling heat transfer of R744 in horizontal small-bore tubes. The result showed that the low surface tension and latent heat also have significant influences on two-phase flow patterns and heat transfer. Huai et al. [10] studied the flow boiling characteristics of R744 in multiport minichannels in an experiment. The result showed that the pressure drop along the test section is very small, and the two-phase R744 flow exhibits a higher heat transfer coefficient than that of the single-phase liquid or vapor flow. Jiang et al. [11] studied the characteristics of heat transfer for the R744 flow boiling at a low temperature in a minichannel. The result showed that the heat transfer coefficient increases with an increase in the mass flux rate but decreases with an increase in the tubes' inner diameter and saturation temperature, and the boiling heat transfer of R744 has a greater effect on nucleate boiling and highly depends on the heat flux. Zhang et al. [12] studied the flow boiling heat transfer characteristics of R744 in a horizontal minitube in an experiment. The result showed that an increase in the heat flux has a significant effect on enhancing the nucleate boiling heat transfer, while it can also speed up the dry-out process and decrease the starting vapor quality of dry-out. Kim et al. [13] studied the evaporative heat transfer and pressure drop of R744 flowing upward in vertical smooth and microfin tubes with a diameter of 5 mm in an experiment. The result showed that the average evaporation heat transfer coefficients for the microfin tubes were approximately 111–207% higher than those for the smooth tube under the same test conditions, and the PF was increased from 106% to 123%.

Regarding the simulation of R744, there are many studies on supercritical flow heat transfer, but few on boiling heat transfer. Wei et al. [14] used FLUENT software to simulate the flow boiling heat transfer of R744/R290 (50/50) in smooth tubes and microfin tubes with an inner diameter of 4 mm and a length of 1.4 m. The results showed that the convective heat transfer coefficient of microfin tubes is higher than that of smooth tubes. Wu et al. [15] studied the flow boiling heat transfer characteristics of R744/R290 in a horizontal smooth tube with an inner diameter of 2 mm. The initial evaporation temperature range was 0–10 °C, the heat flux was 5–15 kW/m², and the mass flux rate was 200–400 kg/(m²·s). The results showed that the heat transfer coefficient of the mixture was between R744 and R290

and decreased with an increase in the R290 mass ratio, which was directly proportional to the initial evaporation temperature, heat flux, and mass flux rate, and the critical dryness was also proportional to the mass flux rate of R290.

On system performance, Kim et al. [16] carried out theoretical and experimental studies on the application of R744/R134a and R744/R290 in an auto-cascade refrigeration system. The results showed that with an increase in the R744 content, the COP increases and the system high pressure decreases. Sarkar et al. [17] proposed that R744/R600 and R744/R600a should be used for medium- and high-temperature heat pumps and that they should heat and cool at the same time. The results showed that R744/R600a instead of R114 for high-temperature heat pump was a good choice. Niu et al. [18] tested the performance of R744/R290 (71/29 mole fraction) for cascade refrigeration. The results showed that the COP and the cooling capacity were higher than those in the R13 system. Onaka et al. [19] analyzed the application of R744/RE170 in a heat pump water heater system. The results showed that the COP of the system was higher than that of pure R744. In addition, the research on the R744 transcritical cycle system is increasing day by day, and the research focuses mainly on the cooling performance of the R744 transcritical cycle, the R744 compressor, the expander [20–25], and the supercritical R744 [26–32].

In terms of the heat transfer phenomenon, Akram et al. [33] studied the results of the double-diffusion convection of Sisko nanofluids creeping along an asymmetric channel with an inclined magnetic field. The results showed that with an increase in the Dufour and thermophoresis variables, the concentration, temperature, and nanoparticle fraction significantly increase. Khan et al. [34] studied the influence factors on the creeping pumping of fourth-stage fluids in nonuniform channels. The results showed that as the influence of Brownian motion increased, the density of nanoparticles increased, which led to an increase in the fraction of nanoparticles. Athar et al. [35] studied the influencing factors of the creeping propulsion of oldroyd-4 constant nanofluids in asymmetric channels. The results showed that the temperature increased with an increase in Brownian motion and the thermophoresis constraint, while the concentration decreased. Noor et al. [36] studied the forced convection of magnetohydrodynamics (MHD) flow and its heat transfer under forced convection caused by a moving lid in a trapezoidal enclosure. The results showed that with an increase in the Reynolds number and heated length, the forced convection phenomenon became more obvious, and when the simultaneous effects of the moving lid force and heated sources moved away from the surface, the local Nusselt number decreased. Wong et al. [37] evaluated the viscous heating mechanism of Newtonian fluid filled in the cavity under the external force on the top lid by means of numerical simulation. The results showed that compared with the nonslip condition, the lower Reynolds number and larger Prandtl number (with the free-slip effect) can reduce the temperature distribution in the cavity at a faster speed, and the free-slip acted like a lubricant.

Because the multicomponent mixture can form azeotropic only in a certain proportion, none of several mixtures can form azeotropic refrigerant in a specific proportion. According to REFPROP 9.0, it is found that R744 and ethane can form azeotropic refrigerant at a ratio of 77.6/22.4. Because ethane is a flammable and explosive working medium, even if R744 can be used as a good fire-extinguishing agent to inhibit the combustion of ethane, some accidents will inevitably be encountered owing to equipment and operation problems in the experimental process, so some accidents can be avoided by using the numerical simulation method.

To sum up, this paper will conduct a numerical study on the flow boiling heat transfer characteristics of R744 and its azeotropic refrigerant. In addition, the performance of azeotropic refrigerants and R744 used in low-temperature heating systems is analyzed, so as to provide a theoretical basis for the future application of azeotropic refrigerant in system and refrigerant replacement.

2. Numerical Approach

2.1. Geometric Model

In this paper, the flow boiling heat transfer of R744 and its azeotropic refrigerant in a horizontal circular tube is studied. The geometric model is in Figure 1, because of the large amount of computation for the complex boiling flow in the three-dimensional tube grid; in order to save time and reduce the amount of computation, the geometric model is simplified as a two-dimensional rectangular fine tube with a length of 100 mm and a diameter of 1 mm.



Figure 1. Geometric model.

2.2. Mathematical Model

The flow boiling problem of refrigerant in a horizontal pipe belongs to the category of a gas–liquid two-phase flow, which involves complex problems such as flow and heat transfer. The VOF multiphase flow model simulates the gas–liquid two-phase flow and heat transfer of refrigerant by solving the momentum equation, the continuity equation of each phase volume fraction, and the energy conservation equation, and the VOF model can also more accurately track the phase interface, so it is convenient to observe the flow pattern in the pipe [38]. The VOF model is often used to simulate the transient process of bubble formation during refrigerant flow boiling in channels. However, in order to obtain more-accurate flow patterns in a steady-state simulation, VOF is also applicable. Therefore, in this paper, the VOF model is chosen as the multiphase flow model for the steady-state of the flow boiling heat transfer of R744 and its azeotropic refrigerant mixture in a horizontal tube. All governing equations of the VOF model can be described as follows.

2.2.1. Basic Equation

Volume fraction equation:

$$\sum_{q=1}^n \alpha_q = 1 \quad (1)$$

where α_q is the volume fraction of the q phase of the working fluid.

Continuity equation:

$$\nabla \cdot (\rho_q \vec{v}_q) = 0 \quad (2)$$

where ρ_q is the density of the q phase of the working fluid and \vec{v}_q is the velocity of the q phase of the working fluid.

Momentum equation:

$$\nabla \cdot (\rho \vec{v} \vec{v}) = -\nabla p + \nabla \cdot \left[\mu \left(\nabla \vec{v} + \nabla \vec{v}^T \right) \right] + \rho \vec{g} + \vec{F}_{vol} \quad (3)$$

$$\vec{F}_{vol} = \sigma \frac{\sum \alpha_q \rho_q \kappa_q \nabla \alpha_q}{0.5(\rho_1 + \rho_2)} \quad (4)$$

$$\kappa_1 = \frac{\Delta \alpha_1}{|\nabla \alpha_1|} \cdot \kappa_v = \frac{\Delta \alpha_v}{|\nabla \alpha_v|} \quad (5)$$

where p is the pressure; \vec{g} is the acceleration vector of gravity; \vec{F}_{vol} is the volume force; ρ and μ are the density and the viscosity of each calculation unit, respectively; σ is the surface tension coefficient; and κ_q is the interface curvature of the q phase of the working fluid. The

surface tension is the surface force, which can be transformed into volume force by using the CFS (continuum surface force) model in [39].

Energy equation:

$$\frac{\partial}{\partial t}(\rho E) + \nabla \left[\vec{v}(\rho E + p) \right] = \nabla \cdot (\lambda \nabla T) + S_E \quad (6)$$

where E is the energy; T is the temperature; λ is the thermal conductivity of the working fluid; and S_E is the energy source term.

2.2.2. Turbulence Model

The RNG κ - ε model is adopted because it is suitable for simulating the complex flow and the high Re (Reynolds number), and the combination of it and the wall function method offers better performance for the near wall flow. The RNG κ - ε model is given in Equation (7). The Reynolds number of R744 is 3571.4–7633.6, and the Reynolds number of the azeotropic refrigerant is 3571.4–8333.3.

$$\begin{aligned} \frac{\partial(\rho k)}{\partial t} + \frac{\partial(\rho k u_i)}{\partial x_i} &= \frac{\partial}{\partial x_j} \left[\alpha_k \mu_{eff} \frac{\partial k}{\partial x_j} \right] + G_k + \rho \varepsilon \\ \frac{\partial(\rho \varepsilon)}{\partial t} + \frac{\partial(\rho \varepsilon u_i)}{\partial x_i} &= \frac{\partial}{\partial x_j} \left[\alpha_\varepsilon \mu_{eff} \frac{\partial \varepsilon}{\partial x_j} \right] + \frac{C_{2\varepsilon}^*}{k} G_k - C_{2\varepsilon} \rho \frac{\varepsilon^2}{k} \end{aligned} \quad (7)$$

where k is the turbulent kinetic energy; ε is the turbulent dissipation rate; u_i is the instantaneous velocity in the rectangular coordinate system; x_i, x_j are the different directions in the rectangular coordinates; μ_{eff} is the effective dynamic viscosity coefficient; G_k is the turbulent kinetic energy due to the time averaged velocity gradient; and $\alpha_k = \alpha_\varepsilon = 1.39$, $C_{2\varepsilon}^* = 1.68$, and $C_{2\varepsilon} = 1.42$.

2.2.3. Interphase Transition Model

On the basis of the phase change evaporation condensation model proposed by Lee in [40], a user-defined function (UDF) program is compiled, which includes the source terms of the mass transfer and the energy transfer. The interphase mass transfer source term m can be described as follows:

$$\begin{aligned} m_{lv} &= r_1 \alpha_1 \rho_1 \frac{T - T_{sat}}{T_{sat}}, T \geq T_{sat} \\ m_{vl} &= -r_v \alpha_v \rho_v \frac{T_{sat} - T}{T_{sat}}, T < T_{sat} \end{aligned} \quad (8)$$

where r_1 and r_v are the interphase heat transfer coefficients, which indicate the heat exchange intensity. In the paper, both r_1 and r_v are set to be 0.1. Too much coefficient will lead to the divergence of numerical calculation, and too little coefficient will cause more deviation in the gas–liquid interface temperature from the saturation temperature.

The interphase energy transfer source term Q can be described as follows:

$$Q = h_{fg} m \quad (9)$$

where h_{fg} is the vaporization latent heat.

2.3. Boundary Condition

In this paper, the velocity inlet boundary condition is selected at the entrance of the pipe, the flow direction is along the positive direction of the x -axis, and the velocity of inlet is calculated by G/ρ . The outlet boundary condition is the outflow boundary condition, and the nonslip for the wall is set as the wall boundary condition. Keep the external boundary of the working fluid flow pipe as a fixed heat flux. The test conditions include the tube diameter (D), the mass flux (G), the heat flux (q), the saturation pressure (P_{sat}), the saturation temperature (T_{sat}), and the specific simulation conditions, which are shown in Table 1.

Table 1. Simulation conditions.

Case	D (mm)	G (kg/m ² ·s)	Q (kW/m ²)	P _{sat} (MPa)	T _{sat} (K)
R744	1	50/75/100	10/20/30	2.3/3.03/3.92	253/263/273
azeotropic refrigerant	1	50/75/100	10/20/30	1.96/2.64/3.47	253/263/273

2.4. Solution Strategy

In this paper, fluent 16.0 is used for the numerical simulation, the VOF multiphase flow model is used to track the gas–liquid interface, the energy equation is opened, the RNG K- ϵ turbulence model is selected, and the wall enhanced wall treatment is checked. Because this paper is based on the steady boiling process to compare the heat transfer characteristics of R744 and its azeotropic refrigerant, the common PISO algorithm has better results for the transient boiling process [40,41], while for the steady boiling process, through continuous calculation, it is found that the flow pattern and the results of the coupled algorithm are closer to the actual situation. The coupled algorithm is used for pressure and velocity coupling; the check coupled with the volume fraction gradient, in discrete options, is selected as the least-squares cell, the pressure is selected as the body force weighted, the volume fraction is selected as compressive, and the rest are selected as second-order upwind. The relaxation factor is selected as the default value.

2.5. The Thermophysical Properties of Working Fluids

Tables 2 and 3 show the thermal properties of R744 and its azeotropic refrigerant at different saturation temperatures; all physical parameters are checked from the software of refprop9.0; and thanks to the fact that the different working fluids have different saturation pressures at the same saturation temperature, this paper only controls the inlet of the R744 and its azeotropic refrigerant, which are saturated liquids with the same saturation temperature.

Table 2. Thermophysical parameters of R744.

Parameter	R744	R744	R744
T _{sat} (K)	253	263	273
ρ_l (kg/m ³)	1032.4	983.7	928.33
ρ_v (kg/m ³)	51.45	70.85	97.18
C _{PL} (kJ/(kg·K))	2.1636	2.3046	2.5377
C _{PV} (kJ/(kg·K))	1.2867	1.5050	1.8578
λ_l (mW/(m·K))	134.82	122.72	110.61
λ_v (mW/(m·K))	15.069	16.928	19.621
μ_l (μ Pa·s)	1.4×10^{-4}	1.2×10^{-4}	1.0×10^{-4}
μ_v (μ Pa·s)	1.31×10^{-5}	1.38×10^{-5}	1.4×10^{-5}
h_{gf} (kJ/kg)	282.78	259	231.35
σ (N/m)	8.62	6.53	4.57
P _{sat} (MPa)	1.96	2.64	3.47

Table 3. Thermophysical parameters of the azeotropic refrigerant.

Parameter	Az-Refrigerant	Az-Refrigerantv	Az-Refrigerant
T _{sat} (K)	253	263	273
Liquid density (kg/m ³)	748.9	704.14	649.59
Vapor density (kg/m ³)	58.99	81.49	114.01
L of specific heat capacity (kJ/(kg·K))	2.5278	2.8231	3.4261
V of specific heat capacity (kJ/(kg·K))	1.7603	2.1978	3.1137
T-conductivity of l (mW/(m·K))	109.53	98.56	87.47
T-conductivity of v (mW/(m·K))	17.54	20.53	25.54
Liquid viscosity (μ Pa·s)	0.9×10^{-4}	0.78×10^{-4}	0.65×10^{-4}
Vapor viscosity (μ Pa·s)	1.2×10^{-5}	1.3×10^{-5}	1.4×10^{-5}
Latent heat of vaporization (kJ/kg)	301.12	276.34	247.42
Tension (N/m)	5.24	3.56	2.03
P _{sat} (MPa)	2.3	3.03	3.92

2.6. Mesh Independent and Method Validation

A quadrilateral grid is used for the computational domain, and it is necessary to study the influence of the grid number on the results. Table 4 shows the local boundary layer grid of three grids, the number of the grid ranges are from 156,104 to 226,228, and the quality of the grid is 1. For the independent verification of the grid size, the working conditions ($G = \text{kg}/\text{m}^2 \cdot \text{s}$, $q = \text{kW}/\text{m}^2$, $T_{\text{sat}} = \text{K}$) are applied to three kinds of grids. Through the simulation, the temperature values at different positions are obtained. Taking the temperature value obtained by the grid number (a) as the benchmark (max relative error of $T = 0$), the maximum temperature error is compared with the other two groups of grids. Table 5 shows the relative error of grids (b) and (c) relative to (a), which are 0.053% and 0.081%, respectively. This shows that when the number of grids is larger, there is no substantial impact on the results. Finally, grid (a) is selected for the following simulation, and the grid division is shown in Figure 2.

Table 4. The local boundary layer grid of three grids.

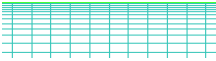
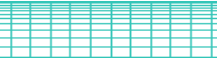
Number of Grid	156,104	182,104	226,228
Grid			
Grid quality	(a) 1	(b) 1	(c) 1

Table 5. Independent verification of grid size.

Number of Grids	Grid Quality	Max Relative Error of T
156,104	1	0%
182,104	1	0.053%
226,228	1	0.081%

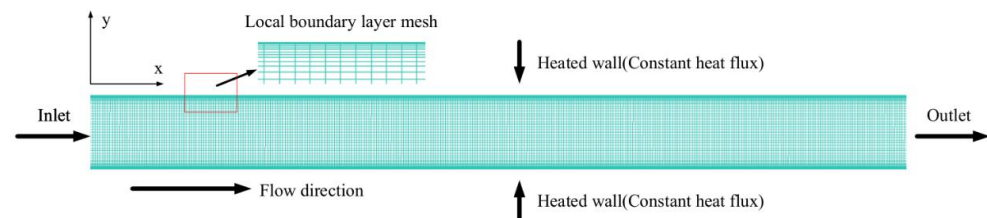


Figure 2. Grid diagram of computing domain.

In order to prove the reliability of the simulation, it is necessary to select the existing experimental data to compare them with the simulation values, but there is no experiment on the flow boiling heat transfer of the R744 azeotropic refrigerant at present. Therefore, the experimental conditions of pure R744 in [5] are selected to compare them with the simulated values of pure R744. Figure 3 shows the change in the flow boiling heat transfer coefficient with dryness. It can be found that the overall trend of the flow boiling heat transfer coefficient between the simulation value and the experimental value is the same, and most of the errors are within the acceptable range. However, there is a large error between the simulation data and the experimental data in the high dryness region, which is caused by the turbulence model, the multiphase flow boiling model, and the algorithm. The simulated values tend to decrease in the high dry area, while there are some special jumping points in the experimental values. In addition, the numerical calculation of the boiling heat transfer under different conditions will have certain deviations, and many research results have shown that the simulation value of the boiling heat transfer coefficient has a large error compared with the experimental value, but this paper focuses on a comparison of the heat transfer characteristics of R744 and its azeotropic refrigerant. Therefore, as long as

the variation law obtained by numerical calculation is consistent with that obtained by the experiment, the simulation result is relatively reliable.

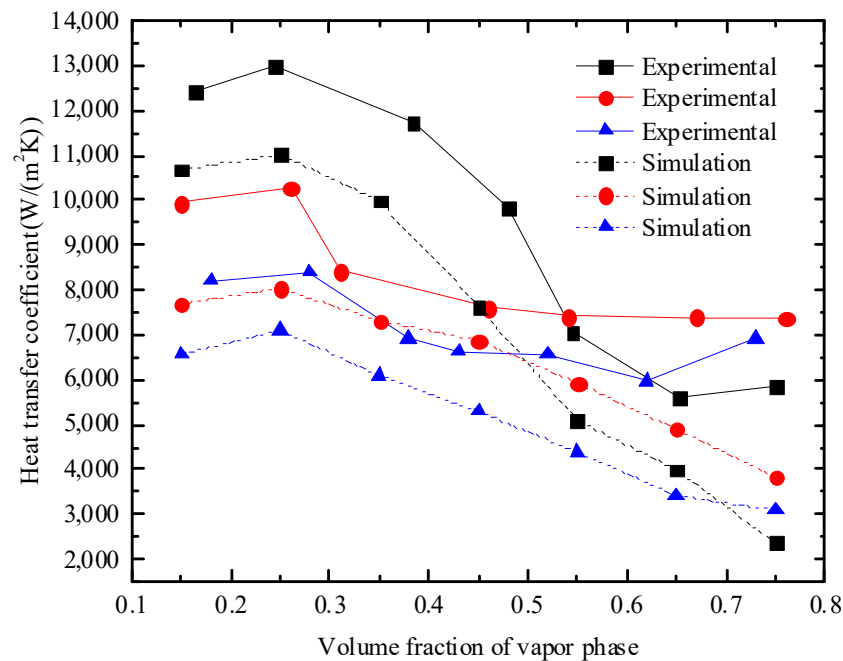


Figure 3. Change in heat transfer coefficient with dryness (the experimental conditions include $D = 6$ mm, $G = 240$ kg/m²·s, $T_{\text{sat}} = 283$ K, and $q = 10$ – 20 kW/m² [7]).

3. Result and Discussion

3.1. Pattern Distribution of Liquid Volume Fraction

Figures 4–9 show the flow pattern of the flow boiling heat transfer of R744 and its azeotropic refrigerant under different working conditions. The evolution process of bubbles from the single-phase flow to the bubble flow and then to the slug flow can be clearly seen. Because of the working conditions, the overall dryness is not high, so the flow pattern reaches only the slug flow.

It can be seen from Figures 4 and 5 that when the mass flux increases, the number of bubbles in the R744 tube decreases. This is because nuclear boiling dominates when the mass flux is small, and the dryness at the same position is larger, so more bubbles can be generated. With the increase in the mass flux, the number of bubbles in the azeotropic refrigerant library seems to first decrease and then increase, but in fact, the bubble flow transitions to the slug flow, and the number of bubbles does not increase.

It can be seen from Figures 6 and 7 that the number of bubbles in R744 and its azeotropic refrigerant tube increases with the increase in the heat flux, which indicates that when the mass flux and the saturation temperature are constant, the boiling phenomenon becomes more intense with the increase in the heat flux.

It can be seen from Figures 8 and 9 that the number of bubbles in the R744 tube first increases and then decreases with the increase in the saturation temperature. This is because when the temperature is between 253 K and 263 K, the number of bubbles increases, which means that the heat transfer effect is better. However, when the bubble decreases from 263 K to 273 K, it means that the heat transfer performance is further improved because there are enough bubbles at 263 K. If the bubbles continue to increase, the tube wall will be dried up. Therefore, the decrease in bubbles represents a further improvement in heat transfer performance. But this phenomenon is not so obvious in the azeotropic refrigerant, which may be related to its physical properties.

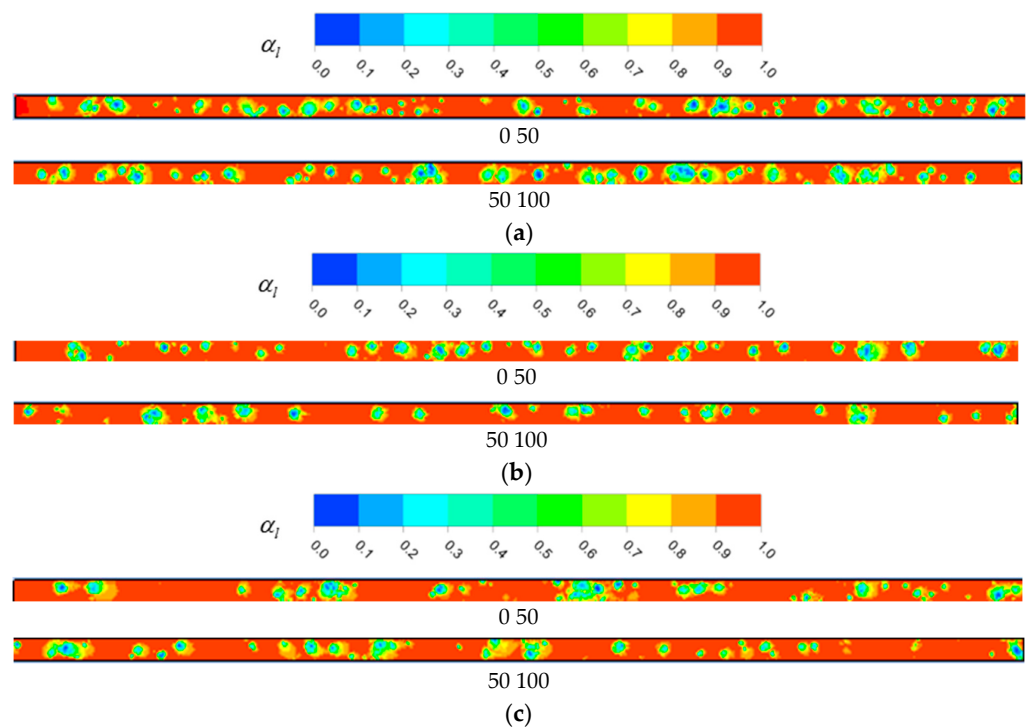


Figure 4. Volume fraction distribution of R744 liquid phase at different mass fluxes: (a) $T_{\text{sat}} = 253$ K, $G = 50$ kg/m²·s, $q = 10$ kW, $X = 0.28$; (b) $T_{\text{sat}} = 253$ K, $G = 75$ kg/m²·s, $q = 10$ kW, $X = 0.19$; (c) $T_{\text{sat}} = 253$ K, $G = 100$ kg/m²·s, $q = 10$ kW, $X = 0.14$.

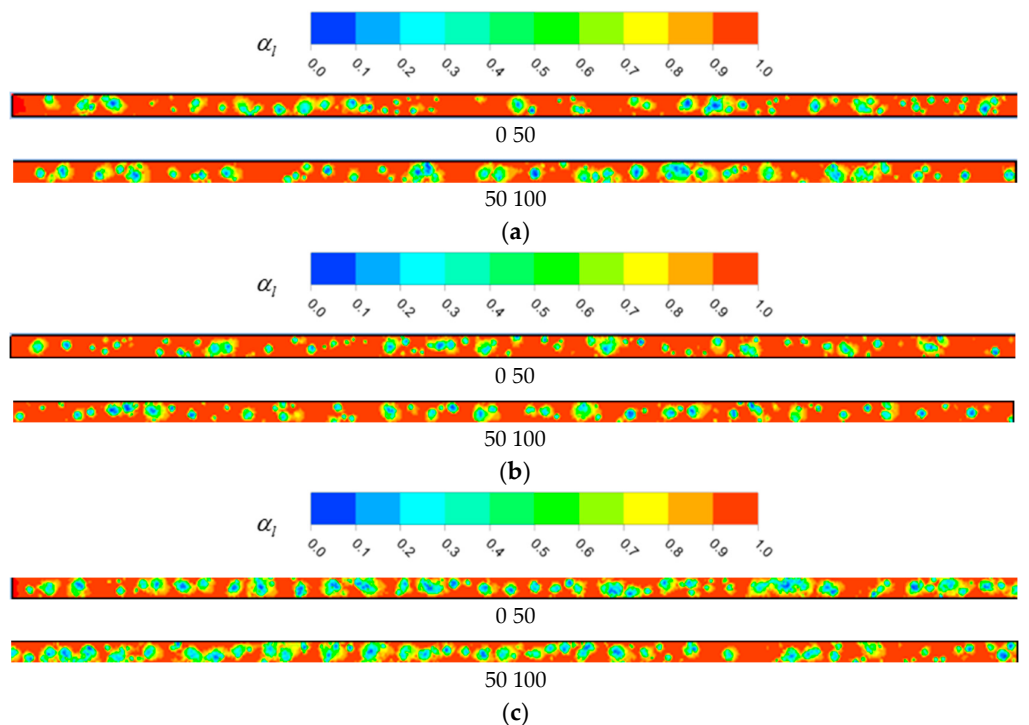


Figure 5. Volume fraction distribution of R744 liquid phase at different heat fluxes: (a) $T_{\text{sat}} = 253$ K, $G = 50$ kg/m²·s, $q = 10$ kW, $X = 0.28$; (b) $T_{\text{sat}} = 253$ K, $G = 50$ kg/m²·s, $q = 20$ kW, $X = 0.56$; (c) $T_{\text{sat}} = 253$ K, $G = 50$ kg/m²·s, $q = 30$ kW, $X = 0.84$.

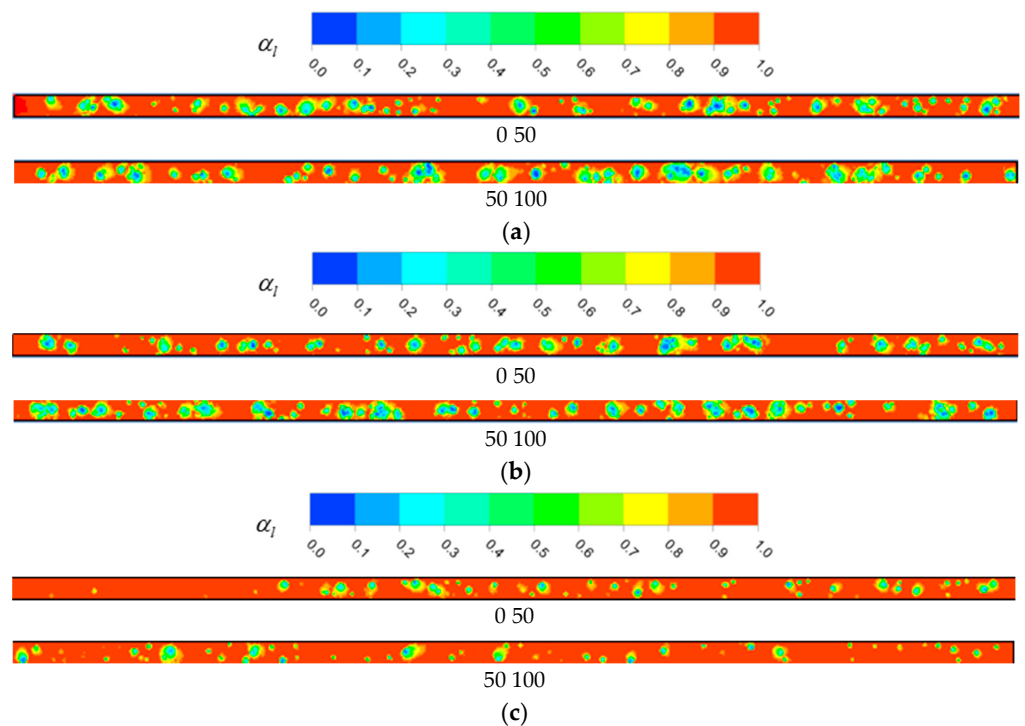


Figure 6. Volume fraction distribution of R744 liquid phase at different T_{sat} values: (a) $T_{\text{sat}} = 253$ K, $G = 50$ kg/m²·s, $q = 10$ kW, $X = 0.28$; (b) $T_{\text{sat}} = 263$ K, $G = 50$ kg/m²·s, $q = 10$ kW, $X = 0.31$; (c) $T_{\text{sat}} = 273$ K, $G = 50$ kg/m²·s, $q = 10$ kW, $X = 0.35$.

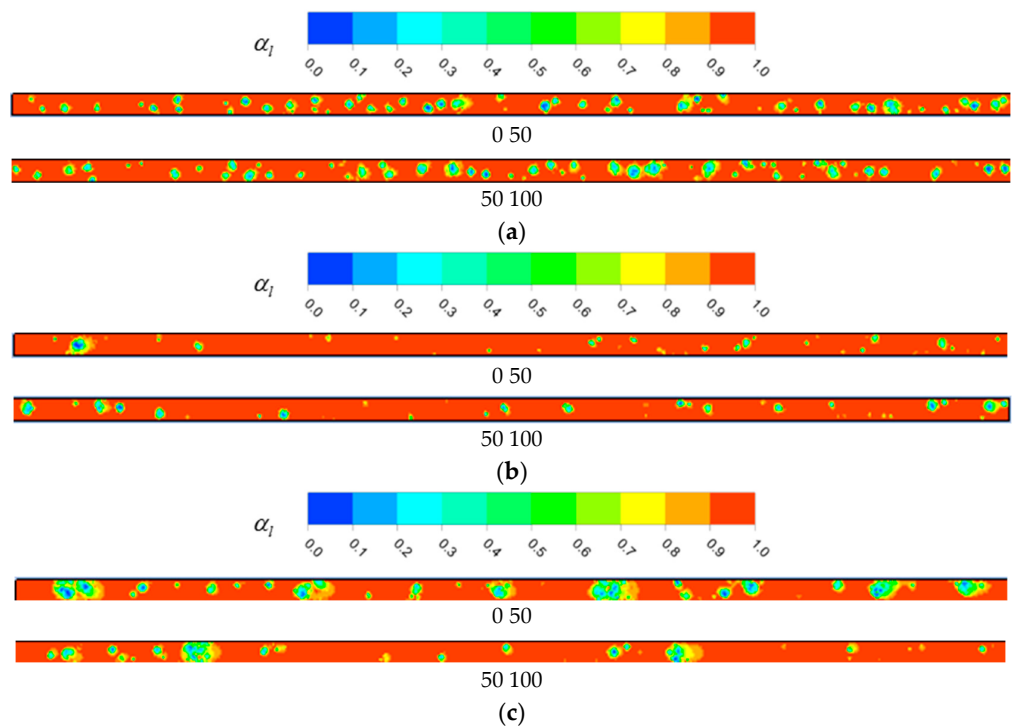


Figure 7. Volume fraction distribution of az-refrigerant liquid phase at different mass fluxes: (a) $T_{\text{sat}} = 253$ K, $G = 50$ kg/m²·s, $q = 10$ kW, $X = 0.26$; (b) $T_{\text{sat}} = 253$ K, $G = 75$ kg/m²·s, $q = 10$ kW, $X = 0.18$; (c) $T_{\text{sat}} = 253$ K, $G = 100$ kg/m²·s, $q = 10$ kW, $X = 0.13$.

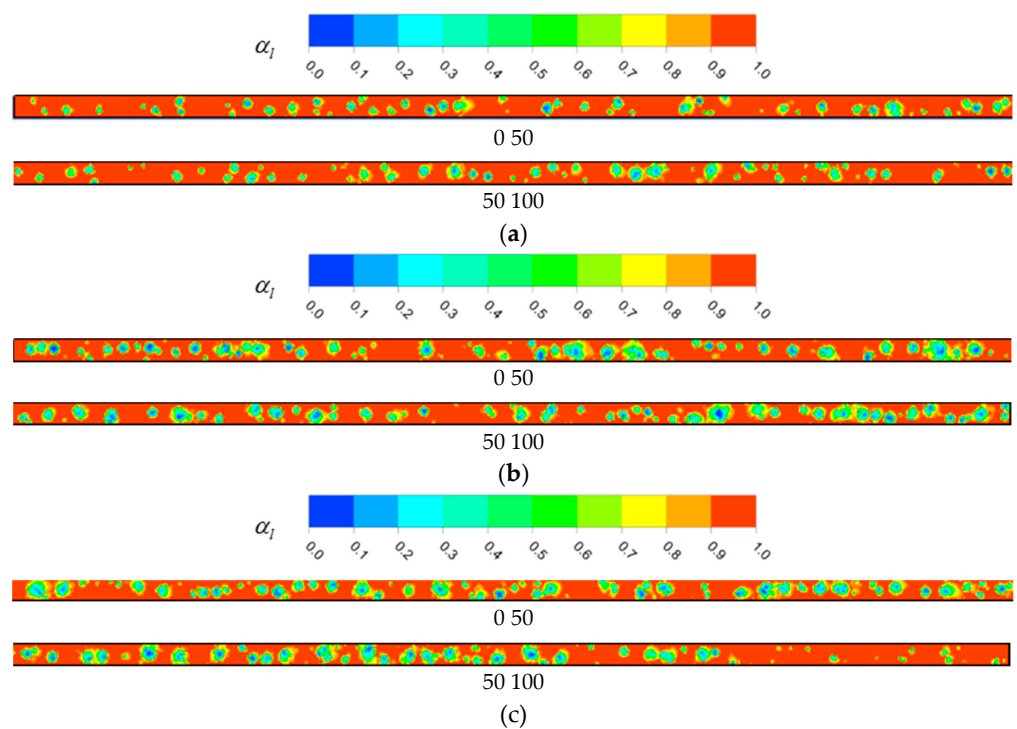


Figure 8. Volume fraction distribution of az-refrigerant liquid phase at different heat fluxes: (a) $T_{\text{sat}} = 253 \text{ K}$, $G = 50 \text{ kg/m}^2\cdot\text{s}$, $q = 10 \text{ kW}$, $X = 0.26$; (b) $T_{\text{sat}} = 253 \text{ K}$, $G = 50 \text{ kg/m}^2\cdot\text{s}$, $q = 20 \text{ kW}$, $X = 0.52$; (c) $T_{\text{sat}} = 253 \text{ K}$, $G = 50 \text{ kg/m}^2\cdot\text{s}$, $q = 30 \text{ kW}$, $X = 0.78$.

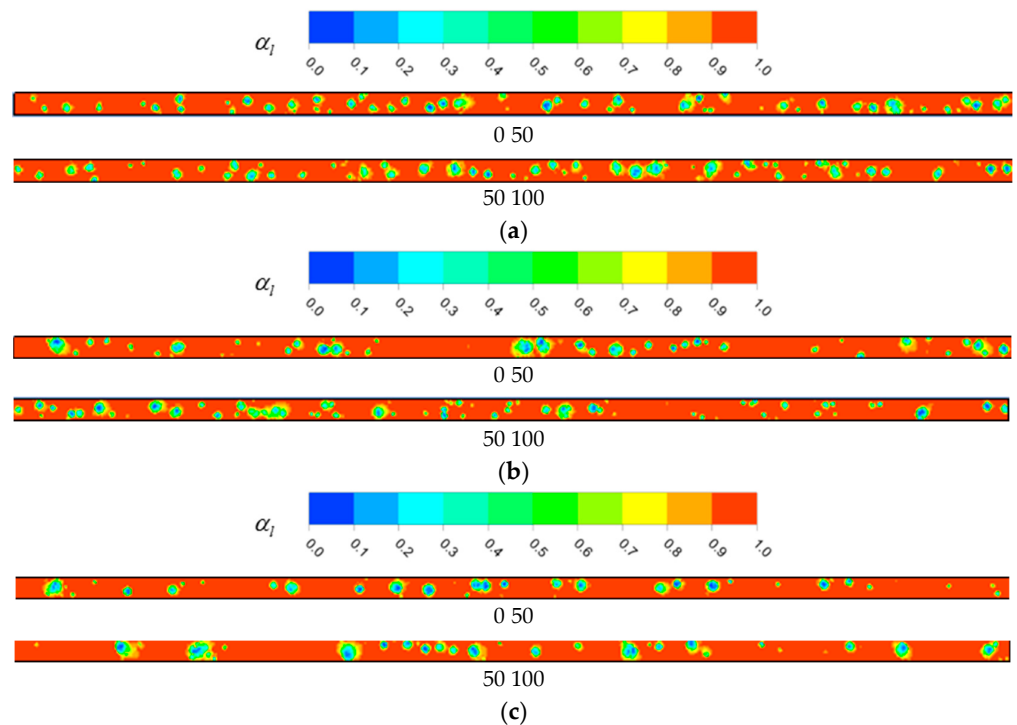


Figure 9. Volume fraction distribution of az-refrigerant liquid phase at different T_{sat} values: (a) $T_{\text{sat}} = 253 \text{ K}$, $G = 50 \text{ kg/m}^2\cdot\text{s}$, $q = 10 \text{ kW}$, $X = 0.26$; (b) $T_{\text{sat}} = 263 \text{ K}$, $G = 50 \text{ kg/m}^2\cdot\text{s}$, $q = 10 \text{ kW}$, $X = 0.29$; (c) $T_{\text{sat}} = 273 \text{ K}$, $G = 50 \text{ kg/m}^2\cdot\text{s}$, $q = 10 \text{ kW}$, $X = 0.32$.

3.2. Effect of Mass Flux on Heat Transfer Coefficient of R744 and Azeotropic Refrigerant

Figures 10 and 11 show the change in the heat transfer coefficient with the quality of R744 and its azeotropic refrigerant under different mass fluxes. It can be seen that the heat transfer coefficient of the azeotropic refrigerant is greater than that of R744 under the same working conditions. This is because from the point of view of the thermophysical properties, at the same saturation temperature, the viscosity of the azeotropic refrigerant is lower than that of R744, and the strong nucleate boiling makes the liquid film on the inner wall of the tube thinner and easier to break. Therefore, the enhancement effect of the low viscosity nucleate boiling on the heat transfer is greater than that of surface tension, and the heat transfer coefficient increases with the increase in viscosity. At the same time, low viscosity is easier to wet the wall with; therefore, the heat transfer performance of the azeotropic refrigerant is better than that of R744.

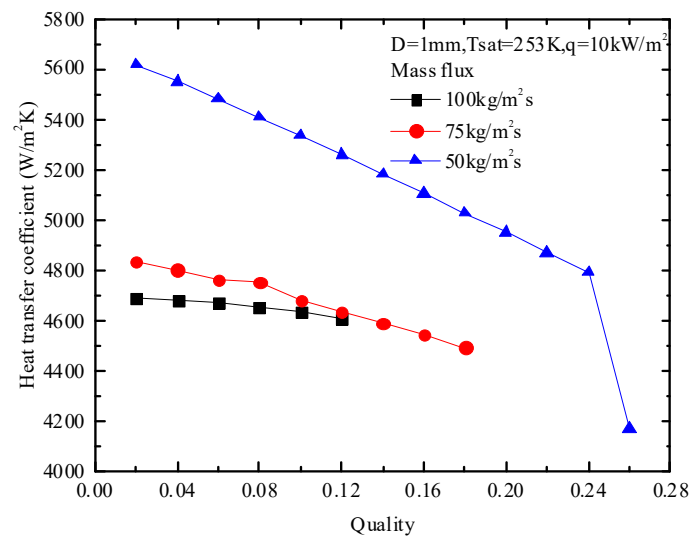


Figure 10. Effect of mass flux on heat transfer coefficient of R744.

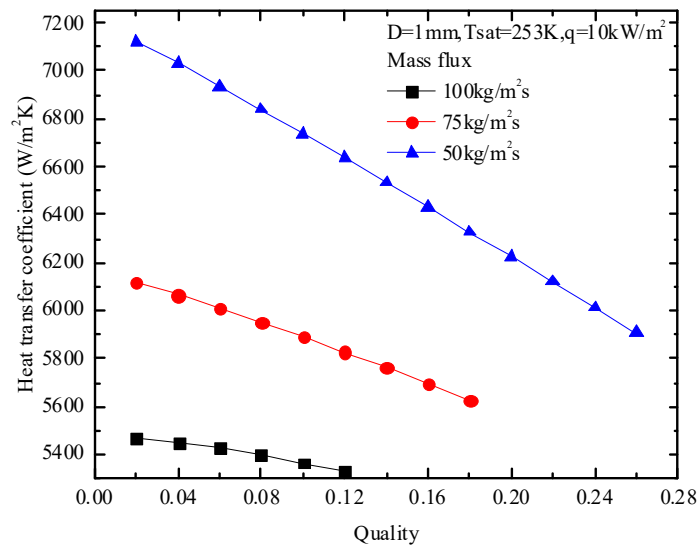


Figure 11. Effect of mass flux on heat transfer coefficient of azeotropic refrigerant.

From Figure 10, we find that the heat transfer coefficient of R744 decreases with the increase in the mass flux. This is because when the mass flux is low, nucleate boiling dominates and the effect is greater than that of the mass flux. However, with the increase in quality, the heat transfer coefficient of the low mass flux sharply decreases. The reason may

be that the wall surface is not timely wetted, owing to the low mass flux, while there is no drying phenomenon at the high mass flux, owing to its low dryness. However, with the increase in quality, the heat transfer coefficient of the high mass flux tends to exceed that of the low mass flux, which is also because the high mass flux can keep wetting the wall and prevent drying up. However, the azeotropic refrigerant did not dry out under the same conditions, which indicated that the occurrence of the dryness of the azeotropic refrigerant was higher than that of R744, which also showed that the heat transfer performance of the azeotropic refrigerant was better than that of R744.

In addition, it can be found from Figures 10 and 11 that within the given quality range, when the mass fluxes of R744 are $50 \text{ kg/m}^2\cdot\text{s}$, $75 \text{ kg/m}^2\cdot\text{s}$, and $100 \text{ kg/m}^2\cdot\text{s}$, the corresponding average heat transfer coefficients are $5137.58 \text{ W/m}^2\text{K}$, $4678.85 \text{ W/m}^2\text{K}$, and $4656.93 \text{ W/m}^2\text{K}$, respectively, and when the mass flux is $50 \text{ kg/m}^2\cdot\text{s}$, the average heat transfer coefficients are 9.8% and 10.3% higher than when the mass fluxes are $75 \text{ kg/m}^2\cdot\text{s}$ and $100 \text{ kg/m}^2\cdot\text{s}$, respectively. Similarly, the corresponding average heat transfer coefficients of the azeotropic refrigerants are $6527.55 \text{ W/m}^2\text{K}$, $5881.89 \text{ W/m}^2\text{K}$, and $5406.93 \text{ W/m}^2\text{K}$; when the mass flux is $50 \text{ kg/m}^2\cdot\text{s}$, its average heat transfer coefficient is 10.9% and 20.7% higher than when the mass flux is $75 \text{ kg/m}^2\cdot\text{s}$ and $100 \text{ kg/m}^2\cdot\text{s}$, respectively. The results show that the heat transfer performance of the azeotropic refrigerant is better than R744, and the increase in its heat transfer coefficient has certain advantages.

Finally, under the given working conditions, when the mass flux of R744 is $50 \text{ kg/m}^2\cdot\text{s}$, $75 \text{ kg/m}^2\cdot\text{s}$, and $100 \text{ kg/m}^2\cdot\text{s}$, its heat transfer coefficient decreases by 25.8%, 7.1%, and 1.7%, respectively, with the increase in quality. The heat transfer coefficient of the azeotropic refrigerant decreases by 17.1%, 7.9%, and 2.5%, respectively.

3.3. Effect of Heat Flux on Heat Transfer Coefficient of R744 and Azeotropic Refrigerant

From Figures 12 and 13, we can find the heat transfer coefficient of R744 and its azeotropic increases with the increase in the heat flux, but it decreases with the increase in quality. This is because the heat flux increases and enhances the nucleate boiling and convective heat transfer, which makes the heat transfer coefficient increase. However, because of the low mass flux, the effect of the convection heat transfer is still less than that of the nucleate boiling, which causes the wall to not be wetted in time, so the heat transfer coefficient decreases. In addition, it is found that the decrease in the heat transfer coefficient at the high heat flux is larger than that at the low heat flux, which is also because the high heat flux intensifies the nucleate boiling, increases the film on the wall, and aggravates the heat transfer deterioration.

In addition, it can be found from Figures 12 and 13 that within the given quality range, when the heat flux of R744 is 10 kW/m^2 , 20 kW/m^2 , and 30 kW/m^2 , the corresponding average heat transfer coefficients are $5137.58 \text{ W/m}^2\text{K}$, $9648.19 \text{ W/m}^2\text{K}$, and $12,688.94 \text{ W/m}^2\text{K}$, respectively, and when the heat flux is 30 kW/m^2 , the average heat transfer coefficients are 146.9% and 31.5% higher than when the heat fluxes are 10 kW/m^2 and 20 kW/m^2 , respectively. Similarly, the corresponding average heat transfer coefficients of the azeotropic refrigerants are $6527.55 \text{ W/m}^2\text{K}$, $12,176.86 \text{ W/m}^2\text{K}$, and $16,017.91 \text{ W/m}^2\text{K}$; when the heat flux is 30 kW/m^2 , its average heat transfer coefficient is 145.3% and 31.5% higher than when the heat fluxes are 10 kW/m^2 and 20 kW/m^2 , respectively. It can be seen that under the influence of different heat fluxes, the increases in their heat transfer coefficients are basically the same.

Finally, under the given working conditions, when the heat flux of R744 is 10 kW/m^2 , 20 kW/m^2 , and 30 kW/m^2 , its heat transfer coefficient decreases by 25.8%, 40.8%, and 61.2%, respectively, with the increase in quality. The heat transfer coefficient of the azeotropic refrigerant decreases by 17.1%, 41.5%, and 61.7%, respectively.

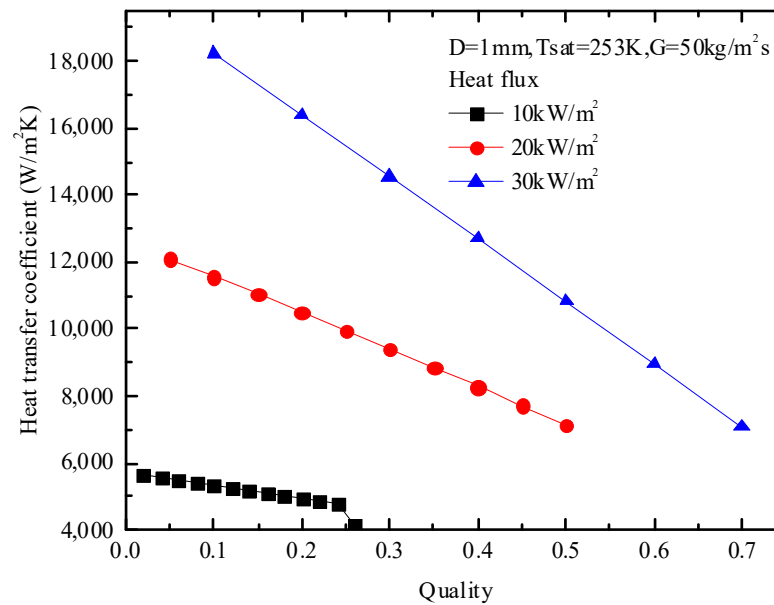


Figure 12. Effect of heat flux on heat transfer coefficient of R744.

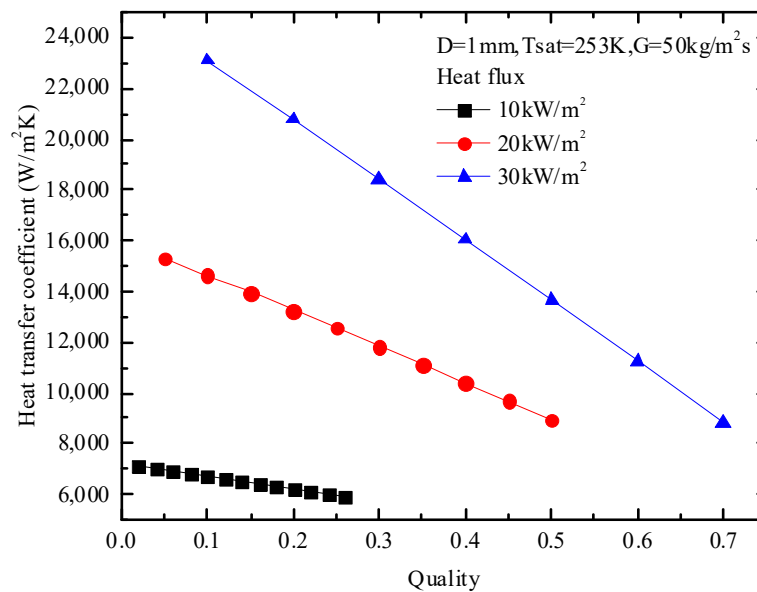


Figure 13. Effect of heat flux on heat transfer coefficient of azeotropic refrigerant.

3.4. Effect of T_{sat} on Heat Transfer Coefficient of R744 and Azeotropic Refrigerant

From Figures 14 and 15, we can find that the heat transfer coefficient of R744 and its azeotropic increases with the increase in T_{sat} because the viscosity of the fluid decreases with the increase in the saturation temperature, and the decrease in the viscosity of the fluid increases the influence of the convective heat transfer, which is conducive to wetting the wall. At the same time, the nuclear boiling makes the liquid film on the inner wall of the tube thinner and easier to break, so the heat transfer coefficient increases when the viscosity is low. In addition, it is found that when R744 is 253 K, the heat transfer coefficient sharply decreases after the quality reaches a certain degree, which is also due to the high viscosity and the earlier drying, resulting in the deterioration of the heat transfer. However, because of the low viscosity of the azeotropic refrigerant increases, there is no sharp decrease in the heat transfer coefficient thanks to the lack of dry-out.

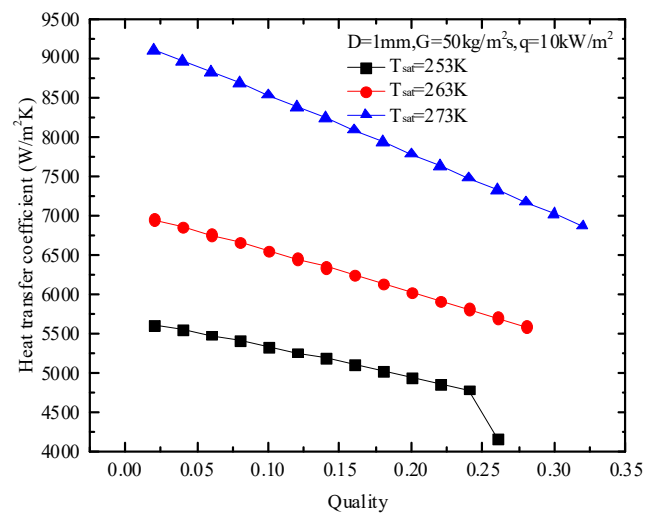


Figure 14. Effect of T_{sat} on heat transfer coefficient of R744.

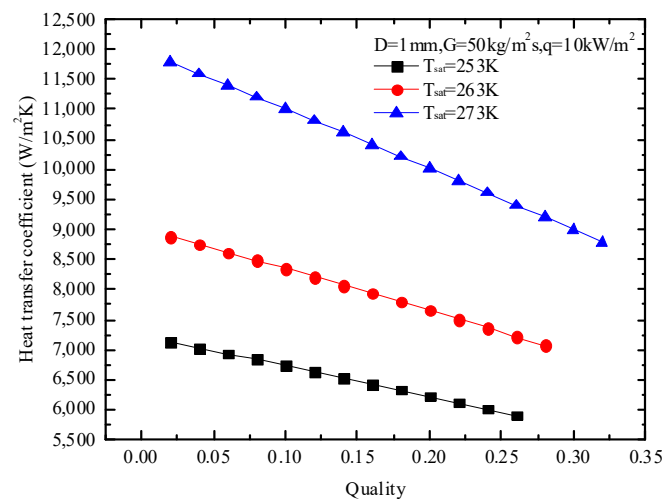


Figure 15. Effect of T_{sat} on heat transfer coefficient of azeotropic refrigerant.

In addition, it can be found from Figures 14 and 15 that within the given quality range, when T_{sat} of R744 are 253 K, 263 K, and 273 K, the corresponding average heat transfer coefficients are 5137.58 W/m²K, 6289.71 W/m²K, and 8004.55 W/m²K respectively, and when the T_{sat} is 273 K, the average heat transfer coefficients are 55.8% and 27.3% higher than when the T_{sat} values are 253 K and 263 K, respectively. Similarly, the corresponding average heat transfer coefficients of the azeotropic refrigerants are 6527.55 W/m²K, 7992.84 W/m²K, and 10,303.96 W/m²K; when the T_{sat} is 273 K, its average heat transfer coefficient is 61.9% and 28.9% higher than when the T_{sat} values are 253 K and 263 K, respectively. It can be seen that under the influence of different T_{sat} values, the increase in the heat transfer coefficient of the azeotropic refrigerants has certain advantages.

Finally, under the given working conditions, when the T_{sat} of R744 is 253 K, 263 K, and 273 K, its heat transfer coefficient decreases by 25.8%, 19.5%, and 24.6%, respectively, with the increase in quality. The heat transfer coefficient of the azeotropic refrigerant decreases by 17.1%, 20.3%, and 25.3%, respectively.

3.5. Comparison of Heat Transfer Performance of R744 and Its Azeotropic Refrigerant

Figures 16–18 show the change in the heat transfer coefficient with the quality of R744 and its azeotropic refrigerant under different working conditions. It can be seen that the greater the heat transfer coefficient of the two, the greater the difference between them,

indicating that the heat transfer performance of the azeotropic refrigerant is better than that of R744. On this basis, if the heat transfer is enhanced by changing the working conditions, the heat transfer performance of the azeotropic refrigerant will be even stronger in R744. In addition, it can be seen from Figures 16–18 that the boiling heat transfer coefficient of the azeotropic refrigerant is 24.37% higher than that of R744 on average when the heat flux is 10 kW, the T_{sat} is 253–273 K, and the mass flux is 50–100 kg/m²·s. Similarly, when the mass flux is 50 kg/m²·s, the T_{sat} is 253 K, and the heat flux is 10–30 kW; the boiling heat transfer coefficient of the azeotropic refrigerant is 26.61% higher than that of R744 on average. When the mass flux is 50 kg/m²·s, the heat flux is 10 kW and the T_{sat} is 253–273 K; the boiling heat transfer coefficient of the azeotropic refrigerant is 27.73% higher than that of R744 on average.

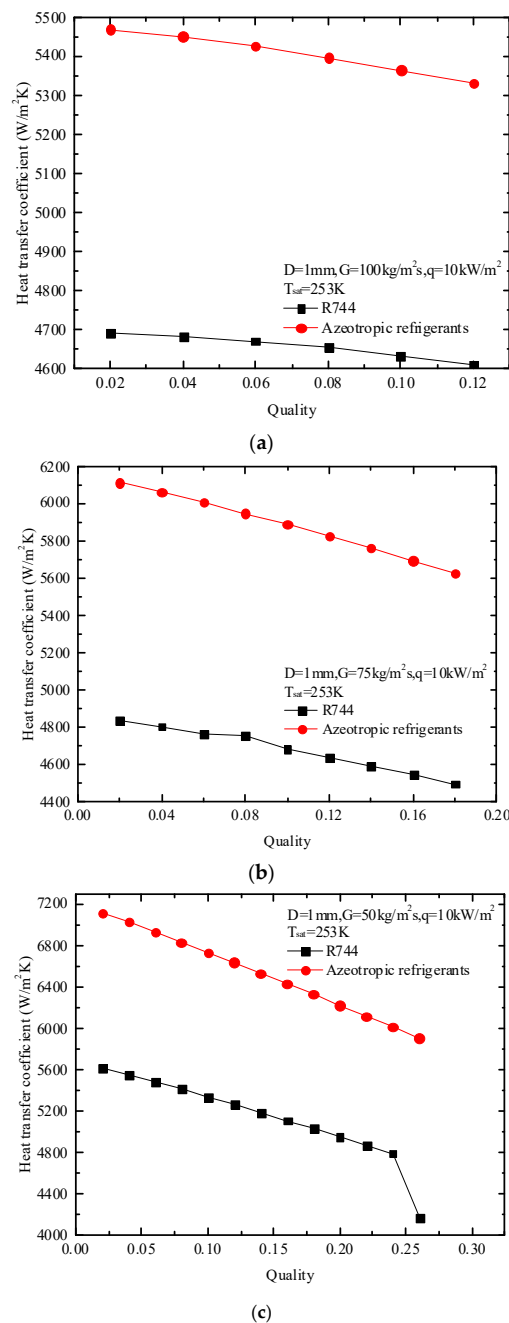
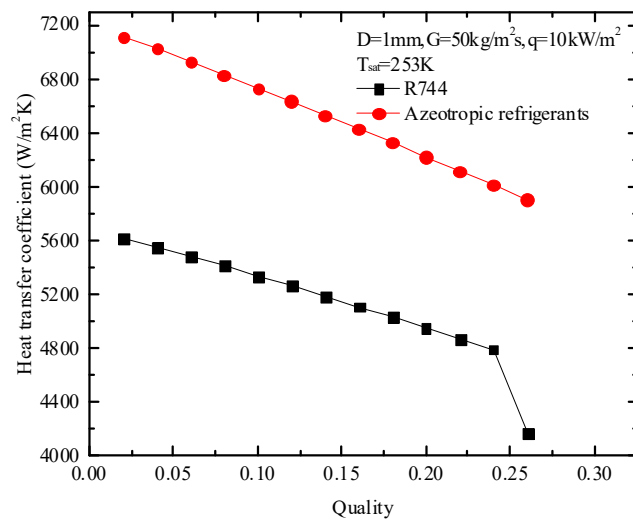
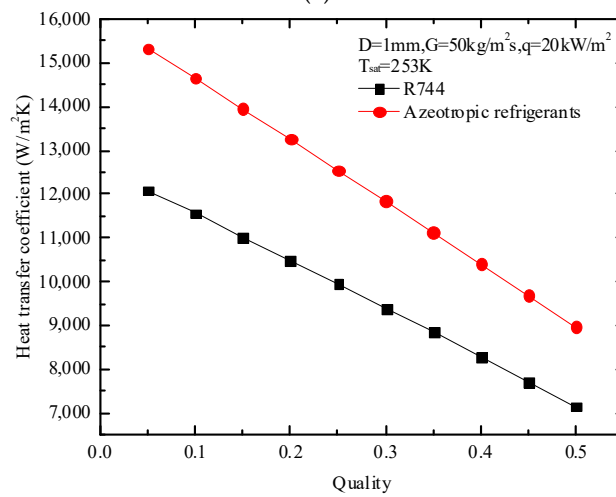


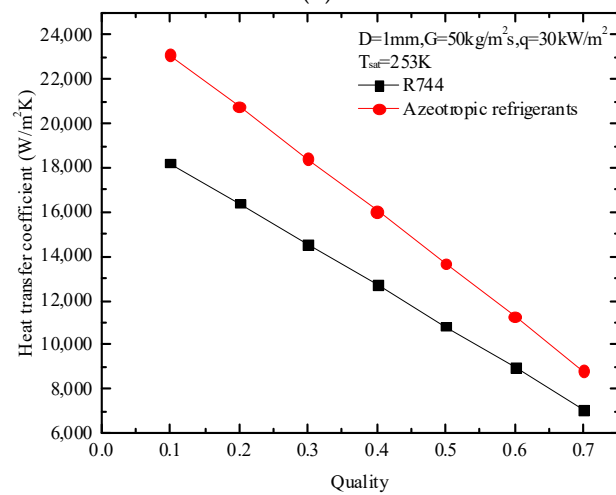
Figure 16. Comparison of heat transfer coefficients between azeotropic refrigerant and R744 at different mass fluxes: (a) $G = 100\text{ kg/m}^2\cdot\text{s}$; (b) $G = 75\text{ kg/m}^2\cdot\text{s}$; (c) $G = 50\text{ kg/m}^2\cdot\text{s}$.



(a)



(b)



(c)

Figure 17. Comparison of heat transfer coefficients between azeotropic refrigerant and R744 at different heat fluxes: (a) q = 10 kW; (b) q = 20 kW; (c) q = 30 kW.

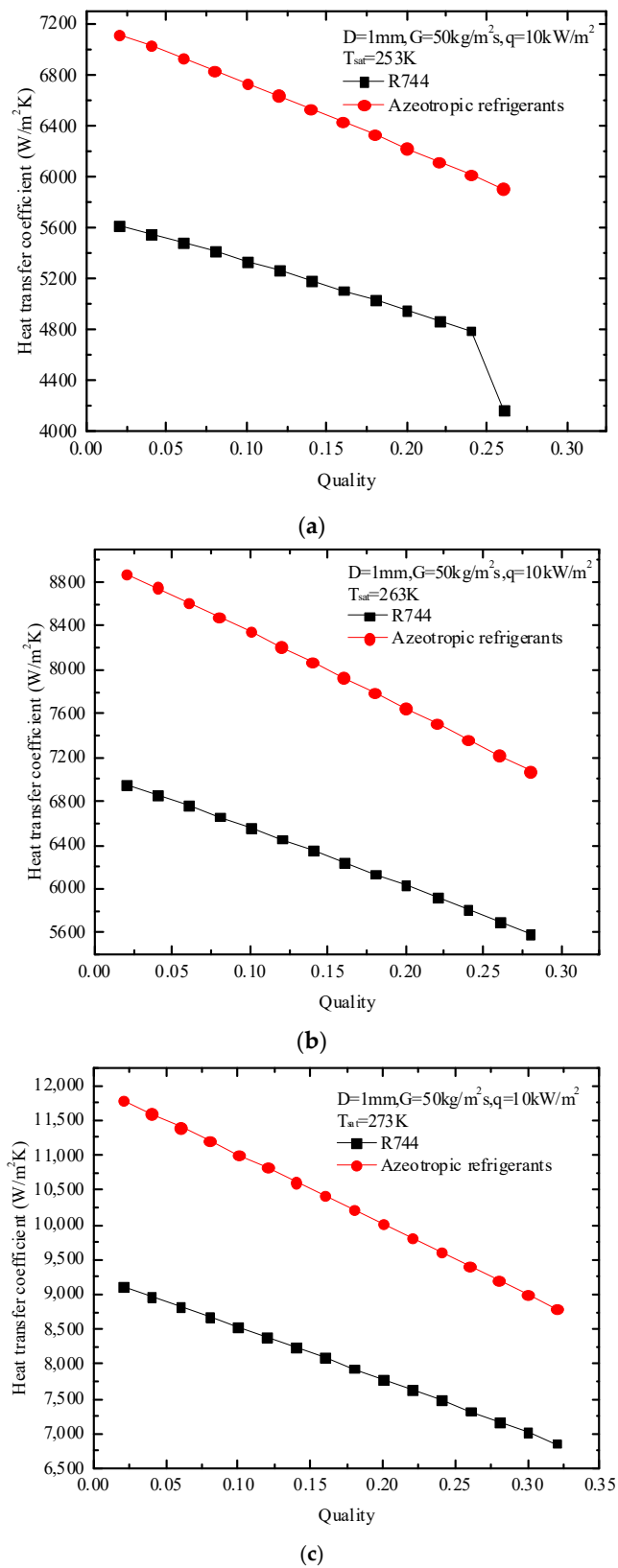


Figure 18. Comparison of heat transfer coefficients between azeotropic refrigerant and R744 at different T_{sat} values: (a) $T_{sat} = 253$ K; (b) $T_{sat} = 263$ K; (c) $T_{sat} = 273$ K.

3.6. Comparison of Low-Temperature Heating System Performance of R744 and Its Azeotropic Refrigerant

In Figure 19, the principle of the subcritical and the transcritical heating cycle systems is demonstrated. The supercritical cycle system uses the large temperature drop in the working medium to exchange heat with the outside world, so it uses a gas cooler instead of a condenser. Figure 20 shows a simple subcritical low-temperature heating cycle: the gas of refrigerant enters the compressor from the evaporator (1); the working fluid is compressed into a high-temperature gas state by the compressor, cooled by sensible heat of 2–3, and then condensed and releases heat by condensation of 3–4 (2); then through 4–5, the condensed liquid phase is led through the pressure relief expansion valve, which reduces the pressure of the liquid and partly evaporates it (3); and finally, the fluid in this state is at its saturation point when it arrives in the evaporator, where it receives heat at low temperatures until it has completely evaporated (4). After this step, the gas is again compressed in the compressor, and the whole cycle is repeated. Figure 21 shows a simple transcritical low-temperature heating cycle: the cycle process is roughly the same as that of the subcritical cycle, but the difference is that the subcritical 2–4 process changes to the 2–3 cooling process with a large temperature drop in the gas cooler, and the state point 3 is unsaturated. Table 6 shows the critical pressure and temperature of R744 and its azeotropic refrigerant. The simulation uses EES software as the calculation tool.

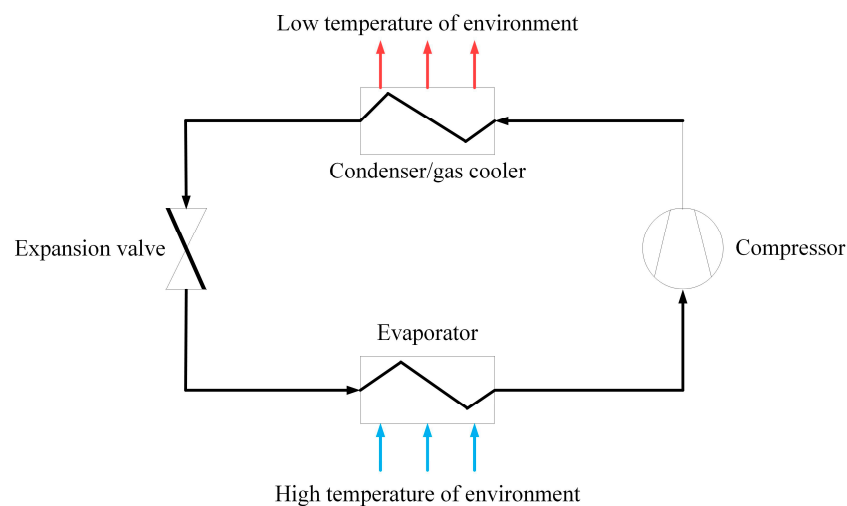


Figure 19. Scheme of the subcritical vapor compression heating working cycle.

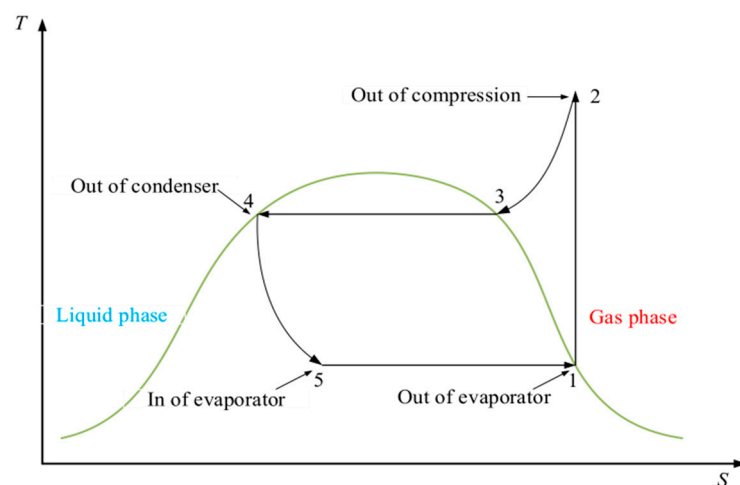


Figure 20. T-S diagram of the subcritical vapor compression heating working cycle.

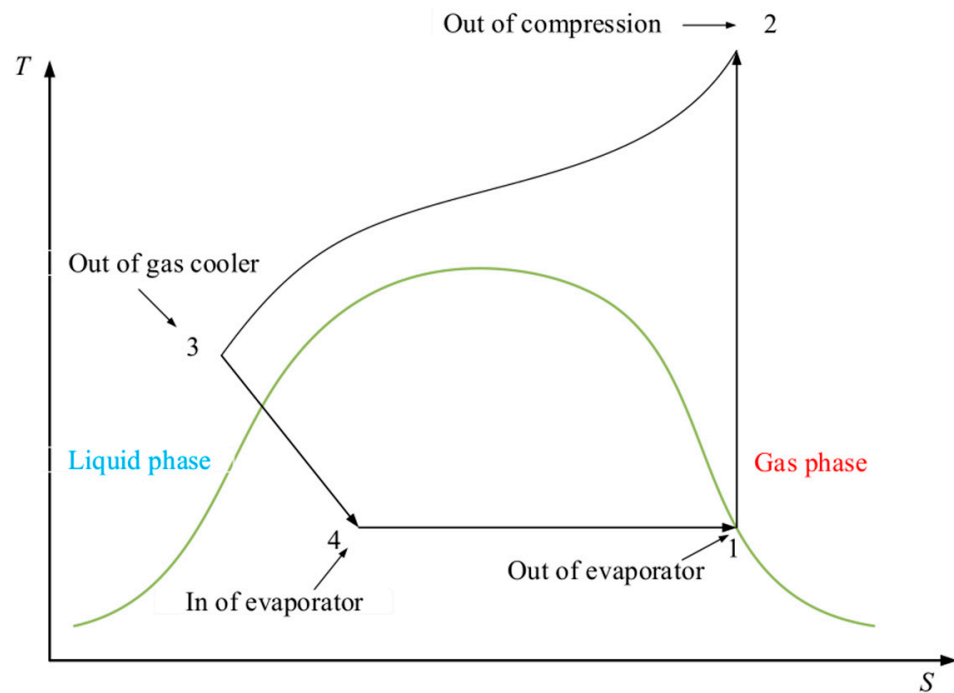


Figure 21. T-S diagram of the transcritical vapor compression heating working cycle.

Table 6. Critical parameters of R744 and azeotropic refrigerant.

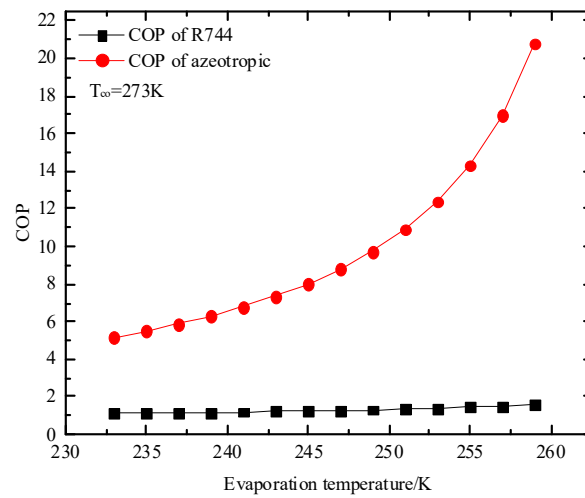
Parameter	Critical Pressure (MPa)	Critical Temperature (K)
R744	7.37	304.13
azeotropic refrigerant	4.87	305.32

Figures 22 and 23 show the variation in the COP and the discharge temperature with the evaporation temperature at a certain condenser outlet temperature in a subcritical system, respectively. The discharge pressure is constant to the saturated pressure of the working medium at the outlet temperature of the condenser.

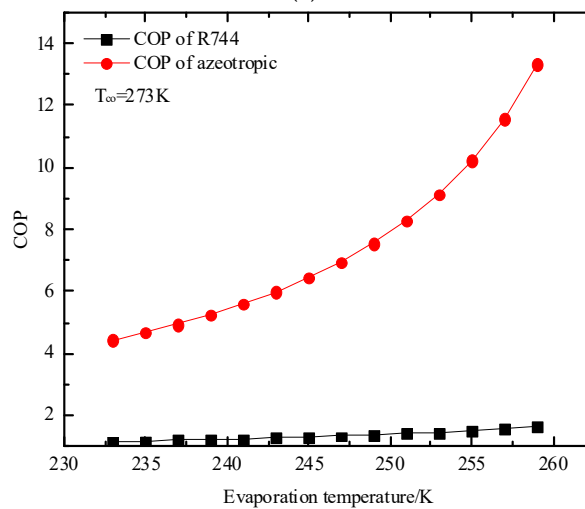
As can be seen from Figure 22, the COP increases with the increase in the evaporation temperature, the COP decreases with the increase in the condensation temperature, which is due to the increase in the evaporation temperature, the increase in suction pressure, and the constant discharge pressure, which leads to the decrease in power consumption and the increase in the COP. It is worth noting that the COP of R744 is lower than that of the azeotropic refrigerant when the outlet temperature of the condenser is low, as shown in Figure 23a,b, and the increase is very small. When the outlet temperature of the condenser is high, as shown in Figure 23c, the COP of R744 is higher than that of the azeotropic refrigerant, and the increase in the COP of the azeotropic refrigerant becomes slow. It can be concluded that the outlet temperature of the condenser is the key factor in determining whether the COP of the azeotropic refrigerant exceeds that of R744.

It can be seen from Figure 23 that no matter how the condenser outlet temperature changes, the discharge temperature decreases with the increase in the evaporation temperature, and the discharge temperature of the azeotropic refrigerant is lower than R744, which indicates that the discharge temperature can be significantly reduced when using the azeotropic refrigerant compared with R744, making the system more stable.

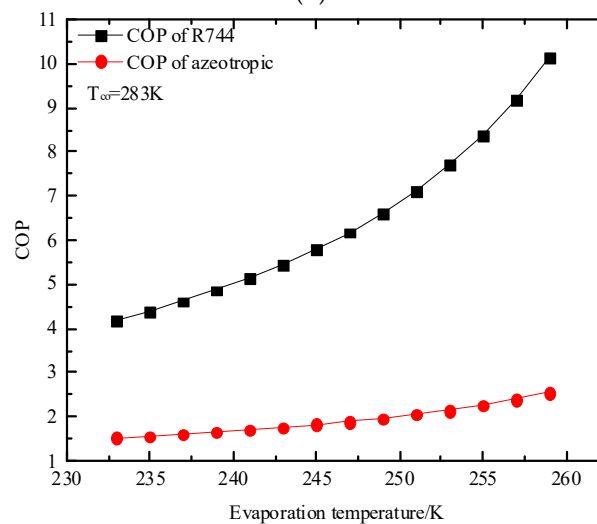
Figures 24 and 25 show the variation in the COP and the discharge temperature with the evaporation temperature at a certain condenser outlet temperature in a transcritical system, respectively. The discharge pressure is 7.5 MPa.



(a)

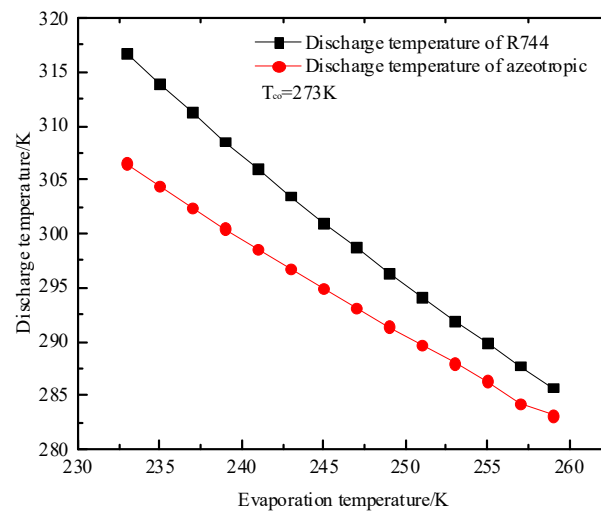


(b)

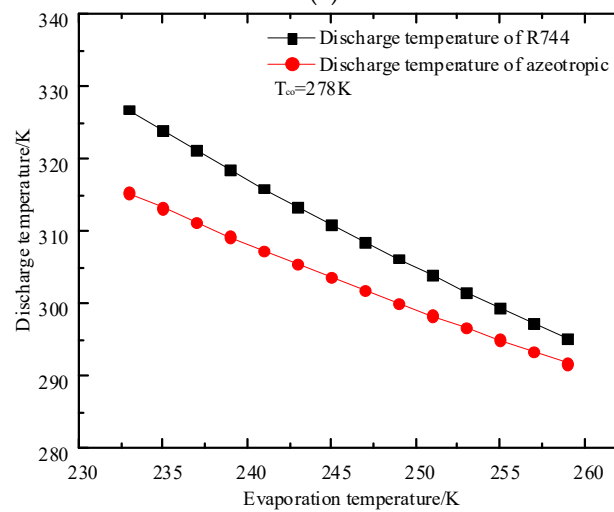


(c)

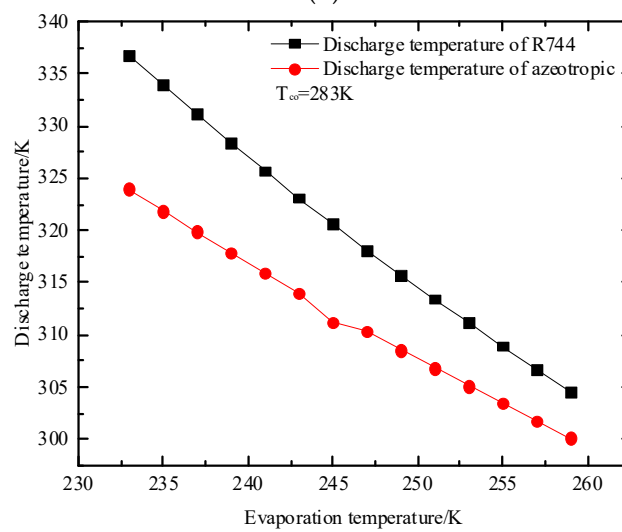
Figure 22. Comparison of COP values of azeotropic refrigerant and R744 varies with evaporation temperature at different outlet temperatures of condenser: (a) $T_{co} = 273\text{K}$; (b) $T_{co} = 278\text{K}$; (c) $T_{co} = 283\text{K}$.



(a)

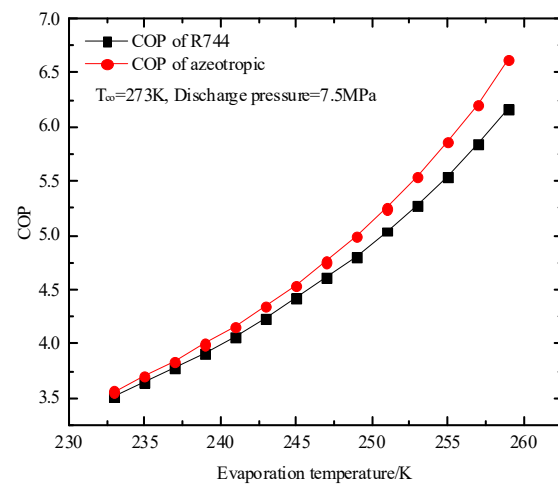


(b)

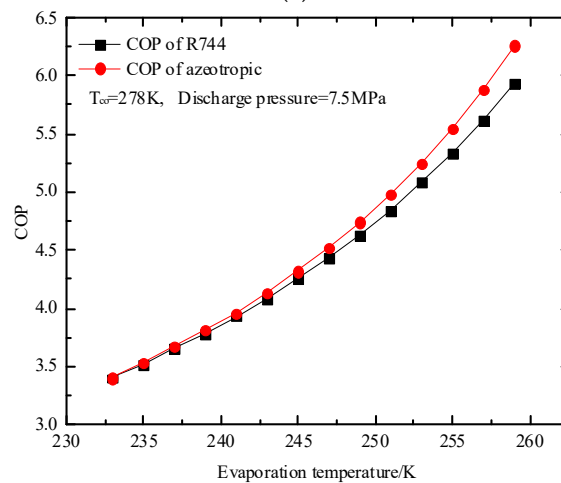


(c)

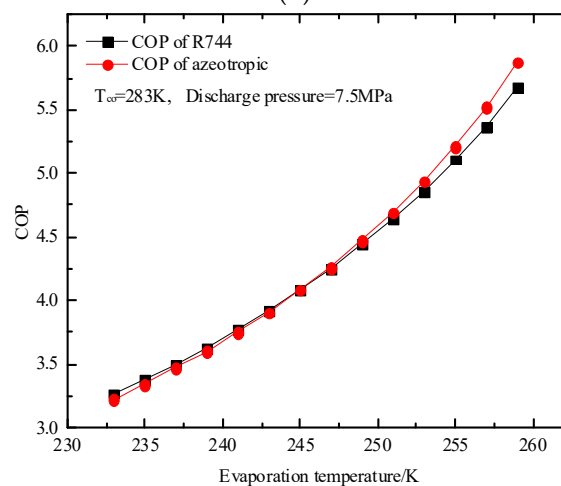
Figure 23. Comparison of discharge temperature of azeotropic refrigerant and R744 varies with evaporation temperature at different outlet temperatures of condenser: (a) $T_{co} = 273$ K; (b) $T_{co} = 278$ K; (c) $T_{co} = 283$ K.



(a)



(b)



(c)

Figure 24. Comparison of COP of azeotropic refrigerant and R744 varies with evaporation temperature at different outlet temperatures of condenser: (a) $T_{co} = 273\text{ K}$; (b) $T_{co} = 278\text{ K}$; (c) $T_{co} = 283\text{ K}$.

The change in the COP with the evaporation temperature is shown in Figure 24 when the discharge pressure is certain. Compared with Figure 22, it is obvious that there is an intersection point between R744 and azeotropic COP (corresponding to the evaporation temperature): the COP of R744 on the left side of intersection will be higher than that of the

azeotropic refrigeration, while the COP of R744 on the right side will be lower than that of the azeotropic refrigeration. We call this intersection the critical point for determining whether the azeotropic refrigerant COP is higher than that of R744. In addition, the position of the critical point is determined by the condenser temperature. The position of the critical point moves to the right with the increase in the condenser temperature, which means that the COP of R744 is higher than that of the azeotropic refrigerant in a given evaporation temperature range. Therefore, if we want to ensure that the COP of the azeotropic refrigerant is higher than that of R744, we need to appropriately reduce the condenser temperature.

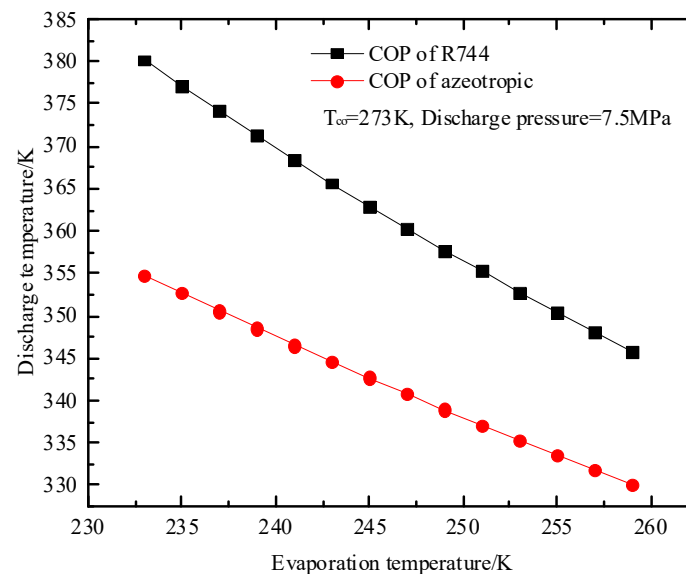


Figure 25. Comparison of discharge temperature of azeotropic refrigerant and R744 varies with evaporation temperature at different outlet temperatures of condenser.

It can be concluded from Figure 25 that the discharge temperature of the azeotropic refrigerant is lower than that of R744 in a subcritical system or a transcritical system, which provides a strong basis for the azeotropic refrigerant to replace R744.

4. Conclusions

In this paper, in order to develop new mixed refrigerant to replace R744, a 2D numerical simulation was established to simulate the flow boiling heat transfer of R744 and its azeotropic refrigerant in a horizontal pipe and then analyze the performance of R744 and its azeotropic refrigerant in the low-temperature heating system. The following conclusions are available:

1. At the low mass flux, the heat transfer coefficients of R744 and its azeotropic refrigerant decrease with the increase in the mass flux.
2. Within a given working condition, the heat transfer coefficients of R744 and its azeotropic refrigerant increase with the increase in the heat flux and the T_{sat} .
3. Under the influence of different factors, the average boiling heat transfer coefficient of the azeotropic refrigerant is 24.37% (mass flux), 26.61% (heat flux), and 27.73% (T_{sat}) higher than R744, respectively.
4. Under the given working conditions, compared with R744, the azeotropic refrigerant is not found to be dry.
5. Compared with R744, the bubble change in the azeotropic refrigerant is more conducive to enhancing the heat transfer.
6. It is found that the critical evaporation temperature makes the COP of the azeotropic refrigerant higher than that of R744.

7. The critical evaporation temperature is determined by T_{CO} , and it increases with the increase in the T_{CO} .

In conclusion, compared with R744, the azeotropic refrigerant has certain advantages in the boiling heat transfer, and by controlling the condensation temperature, the system performance of the azeotropic refrigerant can also be better than that of R744. According to the conclusion of this paper, it has certain reference significance for the replacement research of R744. At the same time, relevant experimental research will be carried out in the future to better understand its heat transfer and system characteristics.

Author Contributions: Conceptualization, D.S.; methodology, D.S.; software, X.Z.; validation, Z.L.; formal analysis, D.S.; investigation, H.Z.; resources, Z.L.; data curation, D.S.; writing—original draft preparation, D.S.; writing—review and editing, D.S. All authors have read and agreed to the published version of the manuscript.

Funding: This research received no external funding.

Data Availability Statement: Data is unavailable due to privacy.

Conflicts of Interest: We declare that we have no financial and personal relationships with other people or organizations that can inappropriately influence our work, there is no professional or other personal interest of any nature or kind in any product, service and/or company that could be construed as influencing the position presented in, or the review of, the manuscript entitled.

Nomenclature

c_p	specific heat at constant pressure (kJ/kg·K)
$C_{2\varepsilon}$	turbulence model's constants
$C_{2\varepsilon}^*$	turbulence model's constants
D	tube diameter (m)
E	energy
F	volume force
g	acceleration due to gravity (m/s^2)
G	mass flux ($kg/(m^2 \cdot s)$)
G_k	turbulent kinetic energy due to time averaged velocity gradient
h	heat transfer coefficient ($W/m^2 \cdot K$)
h_{gf}	vaporization latent heat (kJ/kg)
k	turbulence kinetic energy (m^2/s^2)
m	mass of working fluid (kg)
p	pressure (MPa)
Q	quantity of heat (kW)
q	heat flux (kW/m^2)
Re	Reynolds number
r	interphase heat transfer coefficients
s	source term
T	thermodynamic temperature (k)
v	velocity (m/s)
x	cartesian coordinates (m)
X	quality
Greek symbols	
α	volume fraction
ε	rate of dissipation of k (m^2/s^3)
λ	thermal conductivity ($W/(m \cdot K)$)
μ	dynamic viscosity (Pa·s)
ρ	density (kg/m^3)
σ	tension (N/m)
σ_k	turbulent Prandtl number for k
σ_ε	turbulent Prandtl number for ε
κ	interface curvature

Subscripts

co	outlet temperature of condenser
d	discharge temperature
e	evaporation
eff	effective
l	liquid phase
i,j	general spatial indices
q	phase
sat	saturation
v	vapor phase

Acronyms

R744	carbon dioxide
COP	coefficient of performance
GWP	global warming potential
ODP	ozone-depleting potential

References

- Grauso, S.; Mastrullo, R.; Mauro, A.W.; Vanoli, G.P. R744 and propane blends: Experiments and assessment of predictive methods for flow boiling in horizontal tubes. *Int. J. Refrig.* **2011**, *34*, 1028–1039. [\[CrossRef\]](#)
- Afroz, H.M.; Miyara, A.; Tsubaki, K. Heat transfer coefficients and pressure drops during in-tube condensation of R744/DME mixture refrigerant. *Int. J. Refrig.* **2008**, *31*, 1458–1466. [\[CrossRef\]](#)
- Onaka, Y.; Miyara, A.; Tsubaki, K. Experimental study on evaporation heat transfer of R744/DME mixture refrigerant in a horizontal smooth tube. *Int. J. Refrig.* **2010**, *33*, 1277–1291. [\[CrossRef\]](#)
- Zhu, Y.; Wu, X.; Wei, Z. Heat transfer characteristics and correlation for R744/propane mixtures flow evaporation in a smooth mini tube. *Appl. Therm. Eng.* **2015**, *81*, 253–261. [\[CrossRef\]](#)
- Yun, R.; Kim, Y.; Kim, M.S.; Choi, Y. Boiling heat transfer and dryout phenomenon of R744 in a horizontal smooth tube. *Int. J. Heat Mass Transf.* **2003**, *45*, 2353–2361. [\[CrossRef\]](#)
- Zhao, X.; Bansal, P. Flow boiling heat transfer characteristics of CO₂ at low temperatures. *Int. J. Refrig.* **2007**, *30*, 937–945. [\[CrossRef\]](#)
- Oh, H.-K.; Son, C.-H. Flow boiling heat transfer and pressure drop characteristics of CO₂ in horizontal tube of 4.57-mm inner diameter. *Appl. Therm. Eng.* **2011**, *31*, 163–172. [\[CrossRef\]](#)
- Yun, R.; Kim, Y.; Kim, M.S. Convective boiling heat transfer characteristics of CO₂ in microchannels. *Int. J. Heat Mass Transf.* **2005**, *48*, 235–242. [\[CrossRef\]](#)
- Ozawa, M.; Ami, T.; Ishihara, I.; Umekawa, H.; Matsumoto, R.; Tanaka, Y.; Yamamoto, T.; Ueda, Y. Flow pattern and boiling heat transfer of CO₂ in horizontal small-bore tubes. *Int. J. Multiph. Flow* **2009**, *35*, 699–709. [\[CrossRef\]](#)
- Huai, X.; Koyama, S.; Zhao, T.; Shinmura, E.; Hidehiko, K.; Masaki, M. An experimental study of flow boiling characteristics of carbon dioxide in multiport mini channels. *Appl. Therm. Eng.* **2004**, *24*, 1143–1463. [\[CrossRef\]](#)
- Jiang, L.; Liu, J.; Zhang, L.; Liu, Q.; Xu, X. Characteristics of heat transfer for CO₂ flow boiling at low temperature in mini-channel. *Int. J. Heat Mass Transf.* **2017**, *108*, 2120–2129. [\[CrossRef\]](#)
- Liang, Z.; Linlin, J.; Jianhua, L.; Yue, Z. Investigation of flow boiling heat transfer characteristics of CO₂ in horizontal mini-tube. *Int. J. Therm. Sci.* **2019**, *138*, 109–115. [\[CrossRef\]](#)
- Kim, Y.J.; Cho, J.M.; Kim, M.S. Experimental study on the evaporative heat transfer and pressure drop of CO₂ flowing upward in vertical smooth and micro-fin tubes with the diameter of 5 mm. *Int. J. Refrig.* **2008**, *31*, 771–779. [\[CrossRef\]](#)
- Wei, Z.F.; Wu, X.M.; MO, S.J. Numerical simulation on flow boiling heat transfer of CO₂/propane mixture in tubes with/without micro-fins. *J. Eng. Thermophys.* **2011**, *32*, 1019–1022.
- Wu, X.M.; Zhao, R.; Wei, Z.F.; Huang, X.J.; Wang, W.C. Experimental studies on flow heat transfer of R744/R290 mixture in a horizontal tube. *J. Eng. Thermophys.* **2013**, *34*, 706–709.
- Kim, S.G.; Kim, M.S. Experiment and simulation on the performance of an auto-cascade refrigeration system using carbon dioxide as a refrigerant. *Int. J. Refrig.* **2002**, *25*, 1093–1101. [\[CrossRef\]](#)
- Sarkar, J.; Bhattacharyya, S. Assessment of blends of R744 with butane and isobutane as working fluids for heating applications. *Int. J. Therm. Sci.* **2009**, *48*, 1460–1465. [\[CrossRef\]](#)
- Niu, B.; Zhang, Y. Experimental study of the refrigeration cycle performance for the R744/R290 mixtures. *Int. J. Refrig.* **2007**, *30*, 37–42. [\[CrossRef\]](#)
- Fukuta, M. Performance and characteristics of compressor/expander combination for R744 cycle. In Proceedings of the 7th IIR Gustav Lorentzen Conference on Natural Working Fluids, Trondheim, Norway, 29–31 May 2006.
- Nickl, J.; Will, G.; Quack, H.; Kraus, W.E. Integration of a three-stage expander into a R744 refrigeration system. In Proceedings of the 6th IIR Gustav-Lorentzen Natural Working Fluids Conf, Glasgow, UK, 29 August 2004. 4/A/12.20.

21. Bo, Z.; Xueyuan, P.; Bei, G.; Ziwen, X.; Pengcheng, S. Design and experimental validation of the slider-based free piston expander for transcritical R744 refrigeration cycle. In Proceedings of the 7th IIR Gustav Lorentzen Conference on Natural Working Fluids, Trondheim, Norway, 29–31 May 2006.
22. Huff, H.J.; Radermacher, R.; Preissner, M. Experimental investigation of a scroll expander in a carbon dioxide air-conditioning system. In Proceedings of the 21th International Congress of Refrigeration Washington, Washington, DC, USA, 17–22 August 2003. ICR485.
23. Hua, T.; Yitai, M.; Minxia, L.; Wei, W. Study on Expansion Power Recovery in R744 Trans-Critical Cycle. *Energy Convers. Manag.* **2010**, *51*, 2516–2522.
24. Hua, T.; Yitai, M.; Minxia, L.; Haiqing, G.; Zhongyan, L. Experimental research on impacts of non-condensation gas to expander performance used in carbon dioxide heating. *Appl. Therm. Eng.* **2011**, *31*, 1943–1949. [[CrossRef](#)]
25. Pettersen, J.; Rieberer, R.; Leister, A. Heat transfer and pressure drop characteristics of supercritical carbon dioxide in micro-channel tubes under cooling. In Preliminary Proceedings of the 4th IIR-Gustav Lorentzen Conference on Natural Working Fluids at Purdue, West Lafayette, IN, USA, 25 July 2000; pp. 99–106.
26. Olson, D.A. Heat transfer of supercritical carbon dioxide flowing in a cooled horizontal tube. In Preliminary Proceedings of the 4th IIR-Gustav Lorentzen Conference on Natural Working Fluids at Purdue, West Lafayette, IN, USA, 25 July 2000; pp. 251–258.
27. Liao, S.M.; Zhao, T.S. Measurements of heat transfer coefficients from supercritical carbon dioxide flowing in horizontal mini/micro channels. *Trans. ASME J. Heat Transf.* **2002**, *124*, 413–420. [[CrossRef](#)]
28. Pitla, S.S.; Groll, E.A.; Ramadhhyani, S. New correlation to predict the heat transfer coefficient during in-tube cooling of turbulent supercritical R744. *Int. J. Refrig.* **2002**, *25*, 887–895. [[CrossRef](#)]
29. Pitla, S.S.; Bhatia, K.; Khetarpal, V.; Strikis, G. Numerical heat transfer analysis in heat exchangers for transcritical R744 system. In Preliminary Proceedings of the 4th IIR-Gustav Lorentzen Conference on Natural Working Fluids at Purdue, West Lafayette, IN, USA, 25 July 2000; pp. 307–314.
30. Liao, S.M.; Zhao, T.S. A numerical investigation of laminar convection of supercritical carbon dioxide in vertical mini/micro tubes. *Prog. Comput. Fluid Dyn.* **2002**, *2*, 144–152. [[CrossRef](#)]
31. Zingerli, A.; Groll, E.A. Influence of refrigeration oil on the heat transfer and pressure drop of supercritical R744 during in-tube cooling. In Preliminary Proceedings of the 4th IIR-Gustav Lorentzen Conference on Natural Working Fluids at Purdue, West Lafayette, IN, USA, 25 July 2000; pp. 269–278.
32. Safia, A.; Maria, A.; Khalid, S.; Alia, R.; Metib, A.; Taseer, A. Impact of Partial Slip on Double Diffusion Convection of Sisko Nanofluids in Asymmetric Channel with Peristaltic Propulsion and Inclined Magnetic Field. *Nanomaterials* **2022**, *12*, 2736.
33. Yasir, K.; Safia, A.; Alia, R.; Aewar, H.; Alsulaimani, H.A. Effects of Double Diffusive Convection and Inclined Magnetic Field on the Peristaltic Flow of Fourth Grade Nanofluids in a Non-Uniform Channel. *Nanomaterials* **2022**, *12*, 3037.
34. Athar, M.; Khan, Y.; Akram, S.; Saeed, K.; Alameer, A.; Hussain, A. Consequence of Double-Diffusion Convection and Partial Slip on Magneto-Oldroyd-4 Constants Nanofluids with Peristaltic Propulsion in an Asymmetric Channel. *Complexity* **2022**, *2022*, 7634357. [[CrossRef](#)]
35. Noor, N.F.M.; Haq, R.U.; Wong, H.F.; Alzahrani, A.K.; Ullah, M.Z. Flow and heat transfer due to partially heated moving lid in a trapezoidal cavity with different constraints at inner circular obstacle. *Int. Commun. Heat Mass Transf.* **2022**, *135*, 106111. [[CrossRef](#)]
36. Wong, H.F.; Sohail, M.; Siri, Z.; Noor, N.F.M. Numerical Solutions for Heat Transfer of An Unsteady Cavity with Viscous Heating. *Comput. Mater. Contin.* **2021**, *68*, 319–336. [[CrossRef](#)]
37. Xie, L.; Xie, Y.; Yu, J. Phase distributions of boiling flow in helical coils in high gravity. *Int. J. Heat Mass Transf.* **2015**, *80*, 7–15. [[CrossRef](#)]
38. Brackbill, J.U.; Kothe, D.B.; Zemach, C. A continuum method of modeling surface tension. *J. Comput. Phys.* **1992**, *10*, 335–354. [[CrossRef](#)]
39. Yang, Z.; Peng, X.F.; Ye, P. Numerical and experimental investigation of two phase flow during boiling in a coiled tube. *Int. J. Heat Mass Transf.* **2008**, *51*, 1003–1016. [[CrossRef](#)]
40. Yang, Z.; Peng, X.F.; Ye, P. Numerical study of flow boiling flow patterns and pressure drop of R134a in small tubes under high flight acceleration. *J. Braz. Soc. Mech. Sci. Eng.* **2020**, *42*, 482.
41. Niu, X.; Luo, S.; Fan, L.L.; Zhao, L. Numerical simulation on the flow and heat transfer characteristics in the one-side heating helically coiled tube. *Appl. Therm. Eng.* **2016**, *106*, 579–587. [[CrossRef](#)]

Disclaimer/Publisher’s Note: The statements, opinions and data contained in all publications are solely those of the individual author(s) and contributor(s) and not of MDPI and/or the editor(s). MDPI and/or the editor(s) disclaim responsibility for any injury to people or property resulting from any ideas, methods, instructions or products referred to in the content.